电 化 学
J. Electrochem. 2022, 28(9), 2214010 (1 of 25)

[Review] DOI: 10.13208/j.electrochem.2214010 Http://electrochem.xmu.edu.cn

Recent Development of Low Iridium Electrocatalysts toward Efficient Water Oxidation

Jing Ni[1,2#], Zhao-Ping Shi[1,2#], Xian Wang[1,2], Yi-Bo Wang[1,2], Hong-Xiang Wu[1,2], Chang-Peng Liu[1,2*], Jun-Jie Ge[1,2,3*], Wei Xing[1,2*]

(*1. State Key Laboratory of Electroanalytic Chemistry, Jilin Province Key Laboratory of Low Carbon Chemistry Power, Changchun Institute of Applied Chemistry, Chinese Academy of Sciences, Changchun 130022, China; 2. School of Applied Chemistry and Engineering, University of Science and Technology of China, Hefei 230026, China; 3. Dalian National Laboratory for Clean Energy, Chinese Academy of Sciences, Dalian 116023, China*)

Abstract: Developing high-performance and low-cost electrocatalysts for oxygen evolution reaction (OER) is the key to implementing polymer electrolyte membrane water electrolyzer (PEMWE) for hydrogen production. To date, iridium (Ir) is the state-of-the-art OER catalyst, but still suffers from the insufficient activity and scarce earth abundance, which results in high cost both in stack and electricity. Design low-Ir catalysts with enhanced activity and stability that can match the requirements of high current and long-term operation in PEMWE is thus highly desired, which necessitate a deep understanding of acidic OER mechanisms, unique insights of material design strategies, and reliable performance evaluation norm, especially for durability. With these demand in mind, we in this review firstly performed a systematic summary on the currently recognized acidic OER mechanism on both activity expression (i.e. the adsorbate evolution mechanism, the lattice oxygen mediated mechanism and the multi-active center mechanism) and inactivation (i.e. active species dissolution, evolution of crystal phase and morphology, as well as catalyst shedding and active site blocking), which can provide guidance for material structural engineering towards higher performance in PEMWE devices. Subsequently, we critically reviewed several types of low-Ir OER catalysts recently reported, i.e. multimetallic alloy oxide, supported, spatially structured and single site catalysts, focusing on how the performance has been regulated and the underlying structure-performance relationship. Lastly, the commonly used indicators for catalyst stability evaluation, wide accepted deactivation characterization techniques and the lifetime probing methods mimicking the practical operation condition of PEMWE are introduced, hoping to provide a basis for catalyst screening. In the end, few suggestions on exploring future low-Ir OER catalysts that can be applied in the PEMWE system are proposed.

Key words: oxygen evolution reaction; polymer electrolyte membrane water electrolysis; low-iridium; catalytic mechanism on activity and stability; evaluation criteria for operational stability

1 Introduction

Hydrogen production coupled with renewable energy in polymer electrolyte membrane water electrolyzers (PEMWE) is hailed as the key scheme to enable a decarbonized future[1]. However, its scale-up deployment is plagued by the high system cost derived from the large noble metal usage and poor performance of anodic electrocatalysts toward acidic

Cite as: Ni J, Shi Z P, Wang X, Wang Y B, Wu H X, Liu C P, Ge J J, Xing W. Recent development of low iridium electrocatalysts toward efficient water oxidation *J. Electrochem.*, 2022, 28(9): 2214010.

Received: 2022-07-08, Revised: 2022-07-21. #These authors contributed equally to this work. *Corresponding author, Liu Chang-Peng, Tel: (86-431)85262225, E-mail: liuchp@ciac.ac.cn; Ge Jin-Jie, Tel: (86-431)85262225, gejj@ciac.ac.cn; Xing Wei, Tel: (86-431)85262223, E-mail: xingwei@ciac.ac.cn

oxygen evolution reaction (OER)[2]. Therefore, efforts have been devoted to developing high-performance and low-cost OER catalysts. To date, iridium (Ir) and its oxide still serve as the benchmark OER electrocatalysts in PEMWE with regard to their balance between high activity and durability compared with other candidates[3]. However, the scarce Ir (0.001 ppm in earth's crust, US$60,670 kg^{-1}) greatly hinders its large-scale application[4]. Besides, the disappointing overpotential of OER (usually > 300 mV, orders of magnitude than that of cathode) leads to a significant decrease in the energy efficiency[2]. Therefore, the design of low-Ir catalysts with enhanced performance has become an inevitable trend in the development of PEMWE.

Recently, progress has been made on the development of low-Ir content electrocatalysts, with metal oxide alloys, supported catalysts, spatially structured and single sites catalysts being reported[5]. However, the current catalysts are still suffering from issues including insufficient activity as well as poor stability in a membrane electrode assembly (MEA)[6]. Specifically, the development of low-Ir OER electrocatalysts is regarded highly challenging in the following aspects: (1) The rationale in catalyst design needs to be clarified. The reduction of the amount of Ir calls for establishing a material development strategy based on the clear OER catalytic mechanism to improve the intrinsic activity of each active site, thus boosting the extrinsic performance. (2) The stability of the low-Ir OER catalyst deserves more attention. Although some low-Ir OER catalysts (i.e., single site catalysts) exhibit high OER activity, but their poor stability cannot meet the target of practical applications. Therefore, an in-depth exploration of the activity degradation mechanism is needed to improve durability. (3) Lack of accurate and detailed evaluation protocols for the activity and stability of low-Ir OER catalysts in scalable PEMWE devices has greatly restricted the practicality determination of the electrocatalyst.

In this review, we present a summary on recent advances in tackling the above-mentioned challenges and developing efficient low-Ir OER catalysts over the past few years, with specially focusing on designing high-efficiency low-Ir catalysts based on mechanism and promoting their PEMWE performance. Firstly, the current mechanisms of acidic OER catalysis on both activity and stability are systematically reviewed. Then, the recent developments in low-Ir OER electrocatalysts, including single-site catalysts, multi-metallic alloy oxides, spatially structured catalysts and supported catalysts, are summarized. Thirdly, a survey on evaluation criteria for catalytic stability, both in three-electrode setup and PEMWE single cell, is carried out. In the last, we discuss the remaining challenges and research trends on this topic. It is expected that this review can promote the development of more efficient low-Ir OER catalysts and the commercialization of high-performance PEMWE devices in the future.

2 Catalytic Mechanism on Activity and Stability

2.1 Correlation between OER Catalytic Activity and Stability

The catalytic activity and long-term operational stability are two important aspects that must be considered in the design of acidic oxygen evolution catalysts. However, current research results show these two aspects are intercorrelated, which cannot be tuned independently[7-12]. Based on the analysis on polycrystalline noble metal oxides such as Ru, Au, Ir, Rh, Pt, and Pd (Figure 1a), Karl J. J. Mayrhofer et al.[13] pointed out that the metal dissolution rate, indicative of the inactivation, is positively correlated with the activity (presented in Tafel slope). Similar conclusion was given by Nenad M. Markovic et al.[14] after studying Au, Pt, Ir, Ru and Os (Figure 1b). They believe that this relation is determined not only by the nature of the metal cation, namely the transition of the stable metal cation in the redox state of +4 to the unstable species in higher valence state (i.e., +6 and +8), but also by the density of surface defects. Since amorphous EC-oxides (hydrous oxides formed at high anodic potential) contain more defects, they are more defective than the corresponding crystalline TC-oxides (crystalline thermochemical oxides generated at high tempera-

tures in oxygen). Although the current research focusing on single noble metal oxides, it can be predicted that the relationship between activity and stability is universal, which gives us guidance that suitable catalytic activity and long-term availability in PEMWE can only achieve with balanced activity and durability.

2.2 OER Catalytic Mechanism

The critical role of catalytic mechanism on the catalyst design and performance regulation has motivated tremendous efforts on uncovering the microscopic activity expression process of catalysts. To date, three catalytic routes (Figure 2)[4,5], namely the adsorbate evolution mechanism (AEM), lattice oxygen mediate mechanism (LOM), and multi-active center mechanism, have been proposed and widely accepted.

2.2.1 Adsorbate Evolution Mechanism

Based on density functional theory (DFT), Rossmeisl et al. proposed a widely accepted adsorbate evolution mechanism (AEM) for OER, which involves four concerned proton-electron transfer steps[15, 16]. As shown in Figure 2a, in the typical AEM route, water molecules are adsorbed and activated on the single metal sites, producing three oxygen-containing intermediate species (OH*, O* and OOH*) and four protons coupled with electrons, and finally oxygen

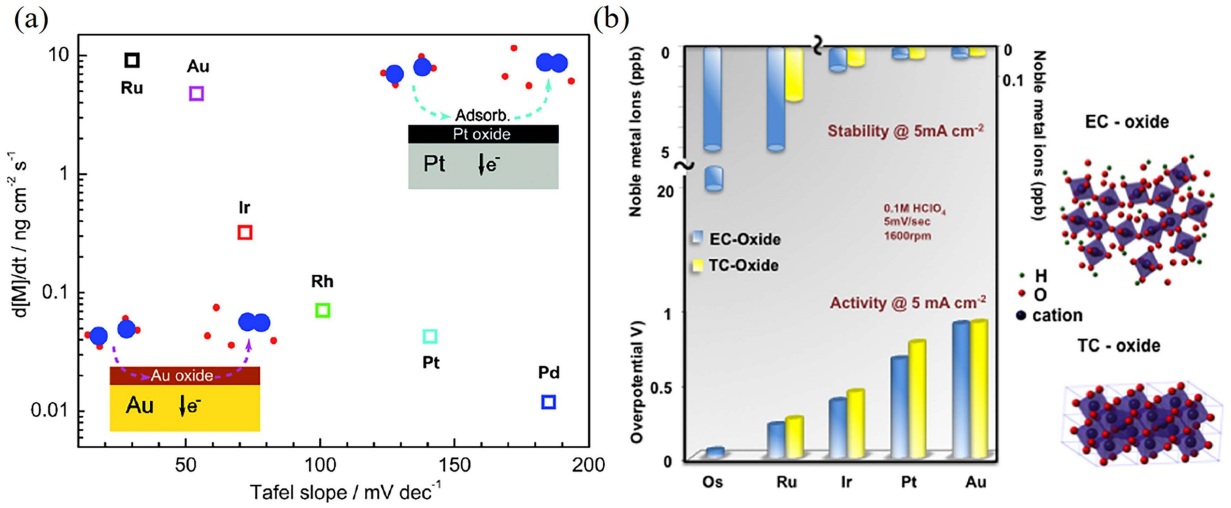

Figure 1 (a) Correlation between activity and stability of polycrystalline metal oxides. Reprinted with permission from rRef.[13], Copyright 2014, Wiley-VCH Verlag GmbH & Co. KGaA, Weinheim. (b) Relationship between activity and stability of single metal oxides, and the effect of their morphology. Reprinted with permission from Ref.[14], Copyright 2014, American Chemical Society. (color on line)

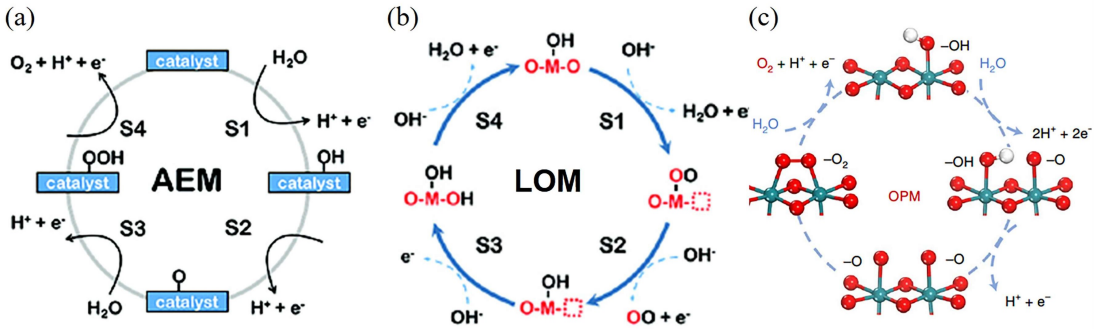

Figure 2 The widely recognized OER catalytic mechanism. (a) AEM; (b) LOM. Reprinted with permission from Ref.[5], Copyright 2020, The Royal Society of Chemistry. (c) OPM. Reprinted with permission from Ref.[4], Copyright 2021, Springer Nature: Nature Catalysis. (color on line)

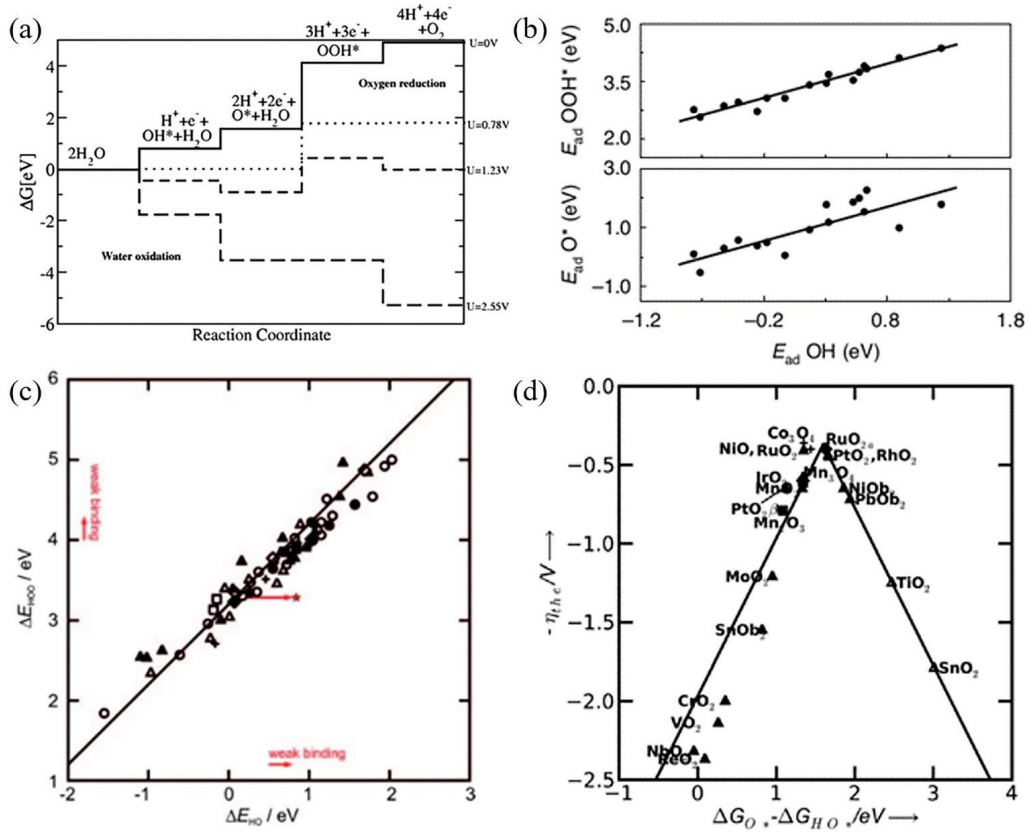

Figure 3 (a) Gibbs free energy diagram under various potentials; Reprinted with permission from Ref.[19], Copyright 2005 Elsevier B. V. (b) Linear relationship of adsorption energies of intermediate oxygen species; Reprinted with permission from Ref.[21], Copyright 2022, Springer Nature: Nature Catalysis. (c) Linear relationship of adsorption energies of intermediate oxygen species; Reprinted with permission from Ref.[15], Copyright 2011, Wiley-VCH Verlag GmbH & Co. KGaA, Weinheim. (d) Theoretical overpotential as a function of OER activity descriptor characterized by the adsorption free energy difference between O* and OH*. Reprinted with permission from Ref.[22], Copyright 2014, The Royal Society of Chemistry.

molecules[17, 18]. The theoretical potential for oxygen evolution is 1.23 V in a standard condition, giving the overall change in Gibbs free energy (ΔG) to be 4.92 eV. In an ideal case, ΔG of every elementary step is the same and equals 1.23 eV, leading to a zero overpotential caused by thermodynamic hindrance. However, the ΔG of each elementary reaction step is not equal in the actual OER catalysis process (Figure 3a)[19]. Generally, the step with maximum ΔG (ΔG_{max}) is defined as the potential-determining step (PDS), that is, the last step able to occur spontaneously with the increase of potential (U)[20].

Based on the thermodynamic analyses, the ΔG of every single proton-electron transfer step can be written as a function of Gibbs free chemisorption energy of two adsorbed oxygen intermediates as shown in Equations 1-4.

$$\Delta G_1 = \Delta G_{HO^*} - \Delta G_{H_2O(l)} - eU + k_bT\ln a_{H^+} \quad (1)$$

$$\Delta G_2 = \Delta G_{O^*} - \Delta G_{HO^*} - eU + k_bT\ln a_{H^+} \quad (2)$$

$$\Delta G_3 = \Delta G_{HOO^*} - \Delta G_{O^*} - eU + k_bT\ln a_{H^+} \quad (3)$$

$$\Delta G_4 = \Delta G_{O_2} - \Delta G_{HOO^*} - eU + k_bT\ln a_{H^+} \quad (4)$$

It is evidenced that the difference in ΔG between each elementary step is caused by the variation in the adsorption energy of different intermediate species. Thus, the catalytic activity is determined by the adsorption strength of different oxygen intermediates. As reported by Jan Rossmeisl et al.[15, 21], there is a general linear correlation between the adsorption energies of O*, HO*, and HOO* (Figure 3b and c). According to the Sabatier principle, the binding between the substrate and the reactant or product should not be too weak or too strong. Only with the appropriate

binding strength can the catalyst have the best activity, thus leading to a volcano type curve of the activity as a function of the OER activity descriptor (Figure 3d)[22].

2.2.2 Lattice Oxygen-Mediated Mechanism

The phenomenon of lattice oxygen participating in oxygen evolution has been observed by Wohlfahrt-Mehrens et al. experimentally as early as in 1987. They detected the isotope oxygen (^{18}O) belonging to the catalyst in the oxygen evolved by differential electrochemical-mass spectrometry (DEMS), which opened the prelude to the research of the anion redox process. Some experimental phenomena, such as the relation between activity and structure of O in the oxide, are well explained by the proposal of the anionic redox process represented by the LOM. Keith J. Stevenson et al.[23] demonstrate that oxygen vacancy defects are a key parameter for improving the electrocatalytic activity of oxygen on metal oxide surfaces. Based on the first-principles calculations, they proposed that lattice oxygen participates in the OER reaction through the reversible formation of oxygen vacancies, and the proposed possible pathway for the oxidation mechanism of lattice oxygen is shown in Figure 2b. Based on DFT principle, Alexie M. Kolpak et al.[24] calculated the adsorption energy and overpotential required for the reaction of a series of perovskite-structured materials via AEM and LOM, with a volcano-shaped curve for the catalytic activity of both the two mechanisms well established. As shown in Figure 4a, the highest theoretical activity performed with LOM is higher than that with AEM, which can be ascribed to the breakage of scaling relation with the participation of lattice vacancy.

To explain the experimentally observed pH-dependent OER activity at the RHE scale, Yang Shao-Horn et al.[25] proposed another possible OER process (Figure 4b), in which lattice oxygen serves as a binding

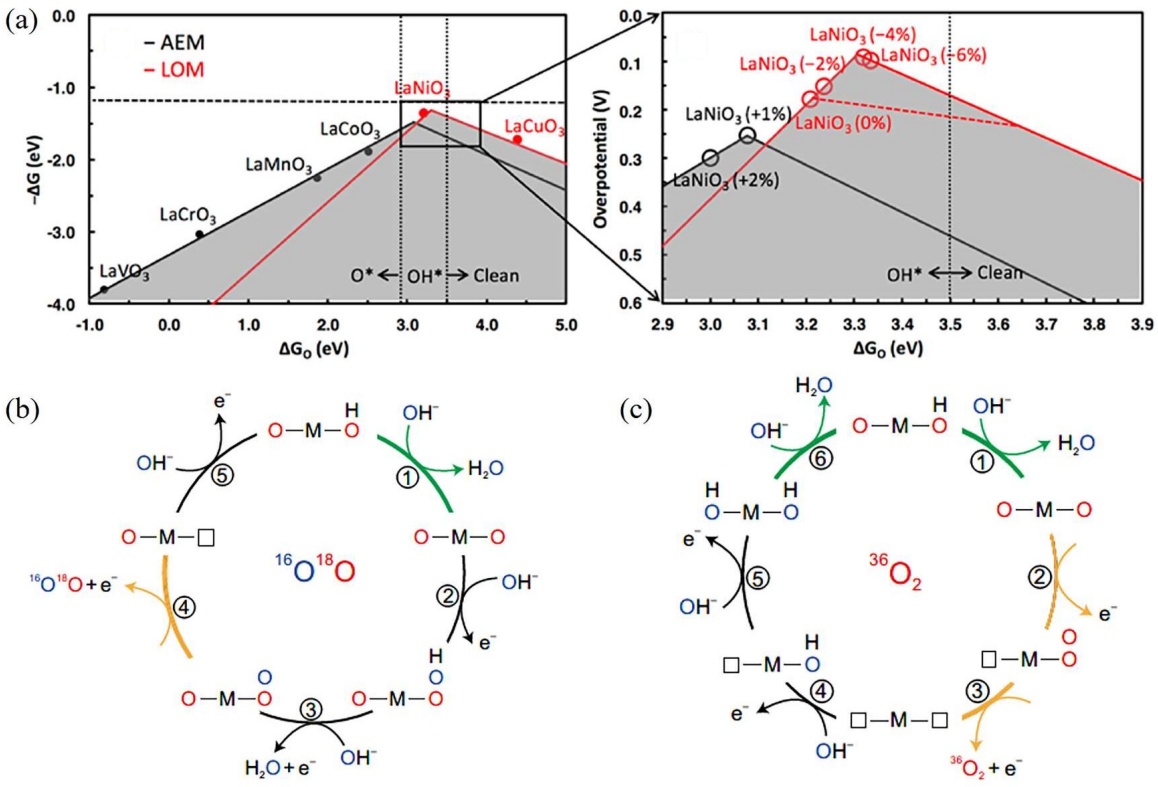

Figure 4 (a) Theoretical overpotential of OER following AEM and LOM; Reprinted with permission from Ref.[24], Copyright 2018, American Chemical Society. (b) Schematic diagram of the OER pathway with lattice as an active site (marked in red); (c) Schematic diagram of the OER pathway in which all oxygen atoms in the gas products come from lattice oxygen. Reprinted with permission from Ref.[25], Copyright 2017, Springer Nature: Nature Chemistry. (color on line)

site for oxygen intermediates, while metal center does not participate in redox chemistry. During this process, lattice oxygen forms O-O bonds with adsorbed oxygen, and then oxygen is released through chemical steps, while oxygen vacancies are created. Furthermore, using *in situ* isotope labeling mass spectrometry, they also found the possibility that all of the oxygen atom in the released O_2 is entirely derived from lattice oxygen. As shown in Figure 4c, lattice oxygen atoms can combine with each other to form O-O bonds, and oxygen molecules are generated while leaving two oxygen vacancies. Since some steps in the above two processes are non-cooperative proton-electron transfer steps, the OER activity exhibits pH dependence at the RHE scale.

2.2.3 Multi-Active Center Mechanism

As an alternative of cationic redox processes, the mechanism with two or more cationic active sites, represented by the oxide path mechanism (OPM) (Figure 2c), has attracted attention from the very beginning, especially in earlier studies based on electrochemical kinetic analysis. Recently, with the help of advanced operando synchrotron FTIR (Fourier transform infrared) spectra, researchers gave evidence for the existence of this mechanism[4]. Besides, theoretical computational analysis shows that the dication redox process has many characteristics that distinguish it from the monocation redox process, which is closer to the real situation in some catalysts and more conducive to OER.

Compared with AEM and LOM, OPM is a more ideal catalytic pathway for catalyst design since the OPM allows direct coupling of O-O without generating additional intermediate species such as OOH* and oxygen vacancies that can lead to the dissolution of active species. Hu et al.[26] prepared a nickel-iron oxide catalyst composed of γ-FeOOH nanoclusters covalently attached to γ-NiOOH support. It was found by theoretical calculations that the OER can proceed in the form of multiple active centers within this structure, where Fe acts as an oxygen generating center and the stepped O site on the adjacent γ-NiOOH oxide support acts as a hydrogen acceptor, promoting the oxygen evolution through the synergistic effect of the two sites (Figure 5a).

However, compared with AEM and LOM, the direct coupling process of O-O in the OPM process calls for a suitable distance between the catalyst double sites, thus the direct O-O coupling can proceed smoothly at a lower energy barrier (Figure 5b). Jung-Ho Lee et al.[4] constructed Ru/α-MnO_2 catalysts with α-MnO_2 as a support, where the positions of Ru atoms follow the periodic arrangement of Mn sites in crystalline α-MnO_2, resulting in the formation of small, ordered Ru arrangement that can shift the catalytic route to OPM pathway.

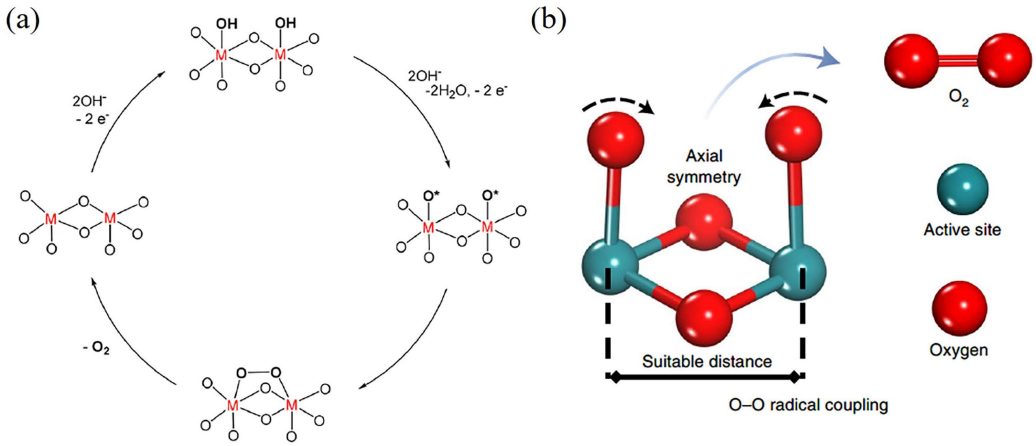

Figure 5 (a) Schematic diagram of the direct coupling pathway of oxygen at the double site; Reprinted with permission from Ref.[26], Copyright 2019, American Chemical Society. (b) Schematic diagram of suitable two-site distance for promoting oxygen release. Reprinted with permission from Ref.[4], Copyright 2021, Springer Nature: Nature Catalysis. (color on line)

2.2.4 Comparison on the OER Catalytic Mechanism

Based on widely accepted reaction pathways, we compare their characteristics and discuss some still-controversial phenomena. As presented in Table 1, differences include the basic catalytic process (cation redox for the AEM and OPM, anion redox for the LOM), limitation of the theoretical overpotential, and the catalytic active sites (one coordinating unsaturated metal ions for the AEM, two CUS with suitable distance for the OPM, and coordinating unsaturated oxygen ions for the LOM). Here we focus on the limitation of the theoretical overpotential, and the widely discussed pH dependency of catalyst activity.

Firstly, the minimum theoretical overpotentials of catalysts under different mechanisms vary. For AEM, the catalytic activity is restricted by the scaling relation between the adsorption energies of OH* and OOH* defined by the bonding nature of oxygen species, giving a minimum overpotential of ~ 0.37 V. While for LOM, the participation of lattice oxygen and formation of vacancies break the scaling relation, thus result in decreased minimum overpotential. According to the study on activities of different types of perovskite catalysts conducted by Yoo et al.[27], the minimum theoretical overpotential of ~ 0.17 V is defined by the step of molecular oxygen formation. However, since there is still no unified understanding of the reaction pathway for the LOM, this minimum theoretical overpotential has not been widely recognized. Similarly, there are also no reports of theoretical overpotentials for the many possible OPM pathways. Secondly, when it comes to the pH-dependent activity, some studies suggest that it is intrinsically related to the reaction mechanism. Namely, the catalytic activity is pH-independent under AEM pathway and pH-dependent under LOM according to the early study performed by Shao-Horn et al.[28] Thus, LOM is also often used to explain the pH-dependent activity of catalysts. However, according to the source of the pH-dependent catalytic activity, i.e., the proton-electron decoupling transfer of the elementary reaction steps, it can be found that the catalyst can exhibit pH-dependent activity even under the AEM pathway. According to the analysis by Coper et al.[29] based on the thermodynamic theory of multi-step electron transfer reactions, only the proton-electron decoupling that occurs at reaction-determining step will have an impact on the performance of the catalyst. Specifically, the decoupling can lead to pH-dependent catalytic activity on RHE scale, showing a value of 59 mV shift per pH, which does not exist in the coupled steps and has become an important evidence to determine this mechanism.

2.3 Stability Mechanism of OER Catalysts

2.3.1 Dissolution of Active Species

The dissolution of catalyst active substances mainly includes two major aspects: chemical dissolution and electrochemical dissolution. First, some substances are dissolved spontaneously in acidic solutions. Some transition metal oxides can react with protons in solutions. For example, Ryuhei Nakamura et al.[30] found that some Mn-based catalysts will be

Table 1 Comparison of the AEM, LOM and OPM pathways.

Mechanism	AEM	LOM	OPM
Catalytic process	Cation redox	Anion redox	Cation redox
Theoretical overpotential	Limited by the scaling relation between OH* and OOH*, minimum value of ~ 0.37 V	Minimum value of ~0.17 V	No related reports
Active site	Single coordination unsaturated metal sites	Single coordination unsaturated oxygen sites	Two coordinations unsaturated metal sites with suitable distance
Identification method	*In situ* attenuated total reflection infrared	Isotope labelled *in situ* differential electrochemical mass spectra	Operando synchrotron FT infrared

dissolved in the acidic medium by the following reactions:

$$Mn_2O_3 + 2H^+ \rightarrow \gamma\text{-}MnO_2 + Mn^{2+} + H_2O \quad (5)$$

$$Mn_3O_4 + 4H^+ \rightarrow \gamma\text{-}MnO_2 + 2Mn^{2+} + 2H_2O \quad (6)$$

In addition, noble metal-based catalysts have also been observed to be dissolved in acidic media. Alexis Grimaud et al.[31] tested the dissolution ratio of metal Ir by inductively coupled plasma (ICP), and found that the Ir-based perovskite will undergo chemical dissolution under acidic conditions, as well as electrochemical dissolution under an applied current (Figure 6a). Via monitoring the oxygen evolution intermediates and degradation intermediates on Ir and its oxide by *in situ* ICP and on-line electrochemical mass spectrometry, Karl J. J. Mayrhofe et al.[32] concluded that the Ir dissolution is closely linked to oxygen evolution, with possible paths illustrated in Figure 6b. Obviously, the dissolution of Ir containing species may occur in three ways, i.e., the direct dissolution of metal Ir, the dissolution through Ir^{V}-Ir^{III} transformation, and the dissolution of IrO_3 at high anodic potential. In addition, another important way of electrochemical dissolution is the lattice oxygen participation in the OER, which can cause the structure collapse and the dissolution of active metal in the form of ions (Figure 6c)[33]. To suppress the dissolution of active species originated from the lattice oxygen participation, strategies as embedding the active site into an oxygen-free substrate, impeding the fast bulk diffusion rates and surface exchange kinetics of atomic oxygen by changing the coordination environment of the active species, and regulating the electronic structure of the active site and the oxygen coordinated. For instance, by embedding active Ru into an oxygen-free NC substrate, Yao et al.[34] demonstrated a high stability of the construct Ru-N-C catalyst with only a 5% performance decay after 30 h of operation. Wu et al.[35] intercalated Ru into a Pt matrix and confirmed that the reaction followed the AEM pathway by *in situ* attenuated total reflection infrared, which is originated from the low contribution of the LOM on metallic Pt and thus sluggish oxygen diffusion. Zhang et al.[36] proposed to construct a Ru-O-Ir local structure with strong interactions to suppress the reactivity of lattice oxygen. Based on quantitative isotope-labeled *in situ* electrochemical differential mass spectrometric analysis, they believe that this localized structure can reduce the participation of lattice oxygen oxidation by ~ 50% and is responsible for the extraordinary operational stability. Although most of these studies have focused on Ru-based catalysts, it is noteworthy that similar problems may occur on Ir-based materials at high oxidation potentials. Therefore, these strategies are also instructive for the construction of stable low-Ir catalysts.

2.3.2 Evolution of Crystal Phase and Morphology

Crystal phase and morphology evolution of the catalyst during OER are also responsible for the perfor-

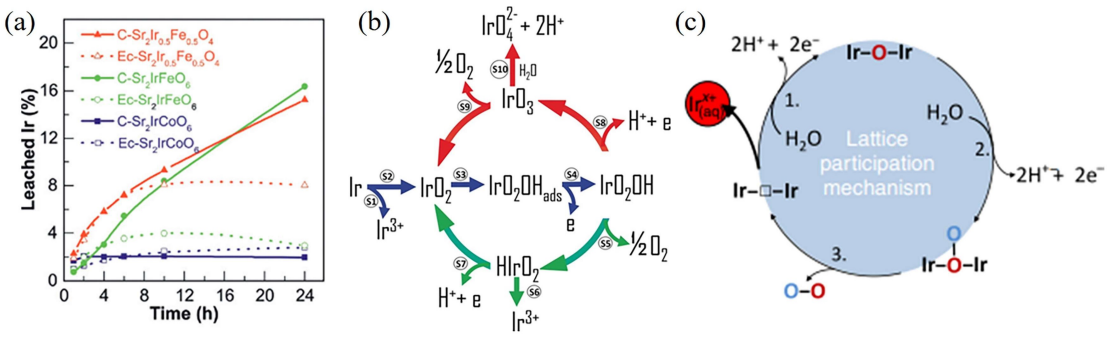

Figure 6 (a) The dissolution ratio of Ir metal during chemical dissolution and electrochemical dissolution of Ir perovskite materials; Reprinted with permission from Ref.[31], Copyright 2019, John Wiley Sons, Inc. (b) The possible Ir dissolution paths, the green line indicates the dissolution path at low point, and the red line indicates the dissolution path under high potential; Reprinted with permission from Ref.[32], Copyright 2018, John Wiley Sons, Inc. (c) Lattice oxygen participates in the reaction path leading to catalyst dissolution. Reprinted with permission from Ref.[33], Copyright 2018, Springer Nature: Nature Catalysis. (color on line)

mance degradation. First, the deactivation can be originated from the loss of active sites due to the agglomeration of the catalyst under the reaction conditions. The work done by Kwangyeol Lee et al. [37] showed that the agglomeration of the Ir/C catalyst occurred during the OER, as shown in Figure 7a. In addition, a surface passivation layer can be formed on some catalysts and thus lead to deactivation at high anode potentials[38, 39]. Specifically, a passivation layer will be formed between the catalyst and the support in two ways: (i) Oxygen species migrate to the interface between the catalyst and the support to form an oxide layer, which increases the electron transfer resistance (Figure 7b, left), (ii) Oxygen species and metal species migrate at the same time then react to form an oxide layer (Figure 7b right). The migration not only leads to the decrease of the conductivity but also the loss of the active sites, thereby deactivating the catalyst. Recently, Linsey C. Seitz et al.[40] found that the $SrIr_{0.8}Zn_{0.2}O_3$ undergoes a metal-to-insulator transition during OER (Figure 7c) and eventually the performance degradation, which is also originated from the structure evolution.

2.3.3 Catalyst Shedding and Active Site Blocking

When performing long-term stability testing, the interaction between the catalysts layer and back electrode substrate also plays a vital role since the weakened interaction will accelerate catalyst fall off and even worse the oxidation of back electrode. After careful investigation on the OER activity and stability of the γ-MnO_2/C catalyst in PEMWE, Ryuhei Nakamura et al. [41] found that the dissolution of carbon black would lead to the exfoliation of the catalyst during OER (Figure 8a). Besides, the catalyst detachment can also be induced by the release of gas at the catalyst/electrode interface[42], thus performance loss.

In addition to causing the exfoliation of catalysts, the release of gas may also block active sites, result

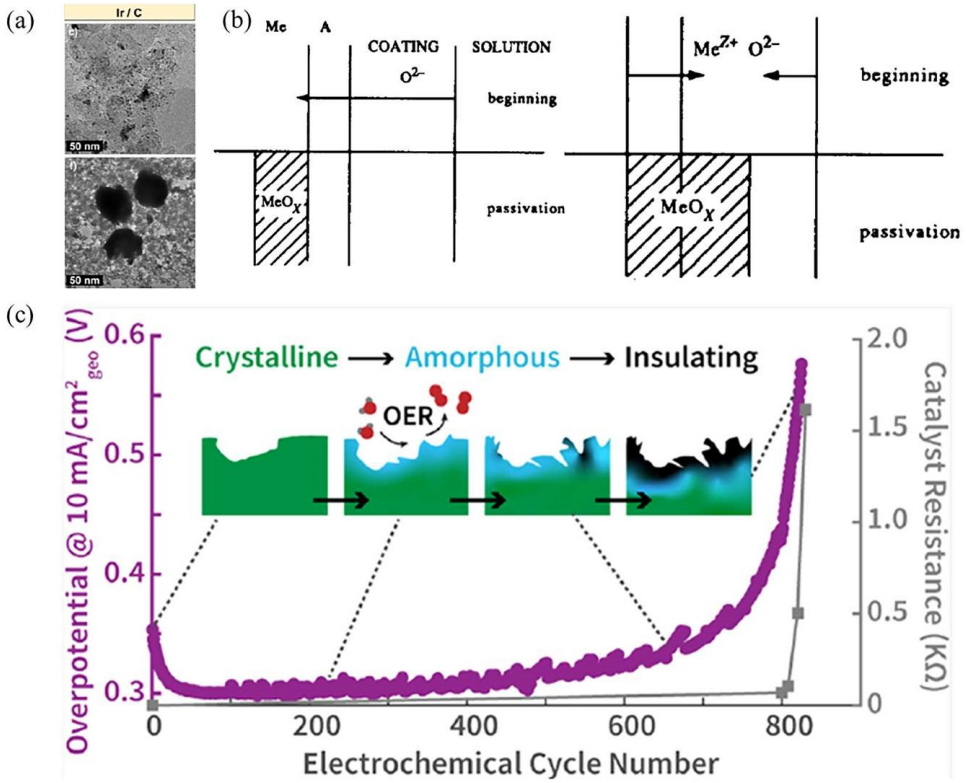

Figure 7 (a) Agglomeration leads to deactivation of Ir/C catalyst. Reprinted with permission from Ref.[37], Copyright 2017, American Chemical Society. (b) Two possible passivation layer formation mechanisms. Reprinted with permission from Ref.[39], Copyright 1994, Elsevier. (c) Schematic diagram of the conversion process of metal to insulator. Reprinted with permission from Ref.[40], Copyright 2021, American Chemical Society. (color on line)

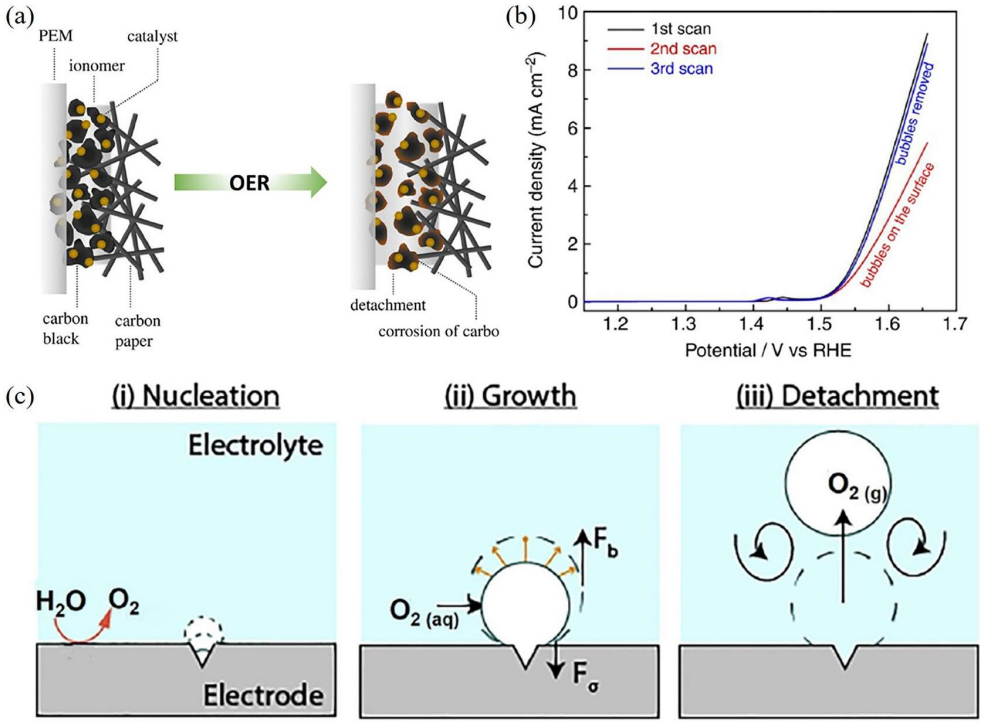

Figure 8 (a) Catalyst shedding due to carbon oxidation; Reprinted with permission from Ref.[41], Copyright 2019, Royal Society of Chemistry. (b) Effect of surface bubbles on electrochemical performance; Reprinted with permission from Ref.[43], Copyright Copyright 2015, Springer Nature: Nature Communications. (c) Diagram of the oxygen production process in the OER process. Reprinted with permission from Ref.[44], Copyright 2020, Elsevier. (color on line)

ing in catalyst deactivation. As shown in Figure 8b, significantly decrease in current density at fix potential can be observed when the surface bubbles are not removed[43]. The formation of bubbles during OER usually involves three steps (Figure 8c): (i) bubble nucleation, (ii) bubble growth and coalescence, and (iii) bubble separation from the catalyst.[44] If the formed bubbles cannot be separated in time, they will block the catalyst surface, separate the catalyst from the electrolyte, prevent ion transport, and lead to catalyst deactivation.

In summary, the causes for performance degradation are complicated, including dissolution of active substance, morphology and structure evolution, catalyst shedding, and active site blocking. The stability of the catalyst is the key performance index that must be considered in catalyst design. Understanding the causes of the performance degradation can help guide the catalyst design by considering the following aspects, (i) avoiding the introduction of soluble elements or inhibiting the dissolution via enhancing the interaction between different components; (ii) developing catalyst with stable morphology and microstructure to avoid the agglomeration and structure collapse during operation; (iii) avoiding the use of carbon-based materials in acid OER catalysts, optimizing the amount of binder (such as Nafion) or constructing self-supported catalysts to delay the shedding of catalyst; (iv) designing the catalyst surface with the suitable bind strength to oxygen molecules so that the generated oxygen can be removed in time.

3 Low-Ir Electrocatalysts

To reduce the amount of precious metal usage without compromising the activity and stability of catalysts, numerous works have been done, with four types of materials, i.e., multimetallic alloy oxides, supported, morphologic controlled and single sites catalysts being widely studied. Herein, we systematically summarize the Ir loading and performance of catalysts with low Ir content reported in recent years,

Table 2 OER activity, types of electrodes, mass loading of typical materials reported in the literature

Catalyst	Electrode	Electrolyte solution	Concentration	Ir loading/ μg·cm^{-2}	Overpotential@ 10 mA·cm^{-2}/ mV	Cell voltage@ 1 A·cm^{-2}/V	Stability	Ref.
Ir-Ni(9.3)	Gold working electrode	$HClO_4$	0.1 mol·L^{-1}	30.6	~ 270			[45]
	Nafion			100		~1.60		
$Cu_{0.5}Ir_{0.5}O_{\delta}$	Ti plate	$HClO_4$	0.1 mol·L^{-1}	~200	~368			[46]
IrCoNi PHNC	GC	$HClO_4$	0.1 mol·L^{-1}	10	303		1 h@5 mA·cm^{-2}	[47]
9R-$BaIrO_3$	GC	H_2SO_4	0.5 mol·L^{-1}	~178	230		48 h@10 mA·cm^{-2}	[48]
Au@$AuIr_2$	GC	H_2SO_4	0.5 mol·L^{-1}	20	261		30 h@10 mA·cm^{-2}	[49]
$IrHf_xO_y$	Au	$HClO_4$	0.1 mol·L^{-1}	~ 0.6	~ 330		6 h@5 mA·cm^{-2}	[50]
Gd-pIrO_2	GC	H_2SO_4	0.5 mol·L^{-1}	278	287		6 h@10 mA·cm^{-2}	[51]
Ir-MoO_3	CP	H_2SO_4	0.5 mol·L^{-1}	~ 77	156		50 h@10 mA·cm^{-2}	[52]
Ir@WO_xNR	W foil	H_2SO_4	0.5 mol·L^{-1}	144	330		10 h@100 mA·cm^{-2}	[53]
	Nafion115			144		1.79	1030 h@0.5 A·cm^{-2}	
IrO_2@Ir/TiN	GC	H_2SO_4	0.5 mol·L^{-1}	379	265		6 h@10 mA·cm^{-2}	[54]
IrO_2@α-MnO_2	Ti plate	$HClO_4$	0.1 mol·L^{-1}	200	275		5 h@10 mA·cm^{-2}	[55]
Ir-Pt-TiO_2	Au	$HClO_4$	0.1 mol·L^{-1}	3.49	> 570		5 h@1.8 V	[56]
	Nafion117			1000		~ 1.90		
IrO_x/ATO	GC	H_2SO_4	0.05 mol·L^{-1}	10.2	~ 430		15 h@1 mA·cm^{-2}	[57]
	Nafion212			1000		~ 1.69		
Ir/Fe_4N	GC	H_2SO_4	0.5 mol·L^{-1}	76.5	316		2 h@10 mA·cm^{-2}	[58]
IrO_2(1:100)-450 ℃	GC	H_2SO_4	0.5 mol·L^{-1}	324	282		2 h@1.56 V	[59]
	Nafion117			1714		1.649		
IrO_2 NN-L	GC	H_2SO_4	1 mol·L^{-1}	214	313		2 h@10 mA·cm^{-2}	[60]
	Nafion117			3428		~ 1.80	250 h@2 A·cm^{-2}	
Ir NF	GC	H_2SO_4	0.05 mol·L^{-1}	200	430			[6]
	Nafion115			200		~ 1.75		
Ir NSs	GC	H_2SO_4	0.5 mol·L^{-1}	137	240		8 h @10 mA·cm^{-2}	[61]
1T-IrO_2	GC	$HClO_4$	0.1 mol·L^{-1}	177	197		45 h@50 mA·cm^{-2}	[62]
	Nafion117			850		1.5 V@ 253 mA cm^{-2}	126@250 mA·cm^{-2}	
3R-IrO_2	GC	$HClO_4$	0.1 mol·L^{-1}	~231	188		511 h@10 mA·cm^{-2}	[63]
$Ir_{0.06}Co_{2.94}O_4$	Au	$HClO_4$	0.1 mol·L^{-1}	~5.2	292		200 h @10 mA·cm^{-2}	[64]
Ir-MnO_2	CP	H_2SO_4	0.5 mol·L^{-1}	192	218		650 h@10 mA·cm^{-2}	[65]
Ir-$NiCo_2O_4$ NSs	CC	H_2SO_4	0.5 mol·L^{-1}	2.44	240		70 h@10 mA·cm^{-2}	[66]
AD-HN-Ir	CP	H_2SO_4	0.5 mol·L^{-1}	3.5	216		100 h@10 mA·cm^{-2}	[67]

focusing on the results not only in three-electrode setups but also in membrane electrode assembly (MEA), as shown in Table 1. Obviously, the optimization of the material design strategy can significantly reduce

the usage of Ir (i.e., to 144 μg·cm^{-2} in MEA) and improve the catalytic performance (i.e., attaining 10 mA·cm^{-2} at 1.386 V). Therefore, in this part, we will discuss these types of low-Ir catalysts, concentrating on how the performance has been regulated.

3.1 Multimetallic Alloy Oxides

Introducing foreign components into a noble metal oxide can not only reduce Ir loading, but also regulate the structure of the active site towards optimized binding strength of oxygen intermediates, thereby improving the intrinsic catalytic activity[2, 68]. To date, Ir-based binary alloy oxides[45, 69], ternary alloy oxides[70], high-entropy alloy oxides[71], and oxides with special crystal structures such as perovskite[72] and pyrochlore[73] have been widely studied. Herein, we pay more attention to how the foreign component modulates the structure, thus the performance of the catalyst, with a special focus on the structure-performance relation.

The foreign component can regulate the electronic structure of Ir via changing the local chemical environment, thereby optimizing its adsorption energy for reaction intermediates. Obviously, direct oxygen-bridge bonding (M-O-Ir) can help modulate the electronic structure of Ir or O (i.e., charge density, d-band center, p-band center, etc.) considering the difference in electronegativity or redox states between M and Ir[74]. Combined with theoretical computation, Hao et al. reported that doping Ta and Tm in IrO_2 can help downward shift the oxygen p-band center and lift the Ir d-band center closer to Fermi level, thus enhancing the binding ability of Ir active sites with oxygen intermediates to boost activity[68]. Recently, a novel Gd doped porous IrO_2 (Gd-pIrO_2) with significantly enhanced activity was reported by our group[51] (Figure 9a and b). We found the valence states of Ir can be tuned by Gd (in +3 valence state) through the charge compensating mechanism. On this basis, a high proportion of Ir^{4+}/Ir^{3+} and facilitating dissociation of hydrogen are obtained by controlling the Gd content (Figure 9c). Besides, Gd ions might broaden the Ir 5d

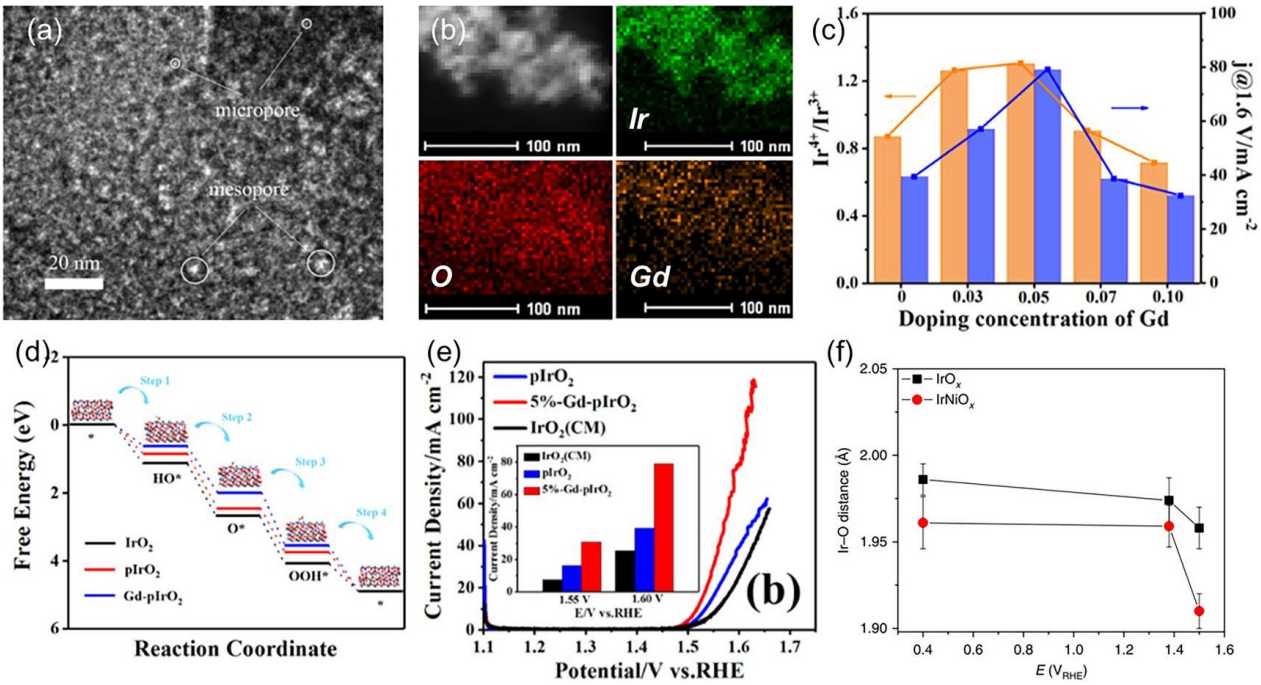

Figure 9 (a) TEM image of Gd-pIrO_2; (b) HAADF-STEM and the corresponding elemental mapping images; (c) Relationship between catalytic activity and proportion of Ir^{4+}/Ir^{3+}; (d) Free energy diagram of the catalytic steps performed on Ir^{4+} sites; (e) LSV curves recorded at a scan rate of 5 mV·s^{-1}, the inset shows the current densities at different applied voltages. Reprinted with permission from Ref.[51], Copyright 2021, American Chemical Society. (f) Effect of cationic vacancy on the Ir-O bond. Reprinted with permission from Ref.[71], Copyright 2018, Springer Nature: Nature Catalysis. (color on line)

bandwidths and strengthen the hybridization between Ir 5d and O 2p orbitals. As a result, the overpotential required to reach 10 mA·cm^{-2} is only 287 mV for Gd-pIrO$_2$, which is 43 mV lower than that of commercial IrO$_2$ (Figure 9d and e). Clearly, it is understandable that changing the foreign element with different physical properties can result in Ir with various structures via direct bonding effect.

In addition to direct bonding, the cation and anion vacancies introduced by foreign components also help in regulating the electronic structure of Ir. Namely, the acid leaching of the unstable components such as Fe, Co, Ni, Zn, etc. can produce a large number of cation vacancies, increasing the content of O^{I-} species and thus promoting the nucleophilic attack of water and formation of the OOH* species[75]. After a careful study of the IrNiO$_x$ system, Strasser et al.[75, 76] pointed out that the cation defects created after Ni leaching lead to an increase in the d-band hole content of adjacent Ir atoms and a shortened Ir-O bond length (thus enhanced covalency, Figure 9f), which can be responsible for enhanced activity. The oxygen vacancy is usually introduced when alloying Ir with foreign elements in low redox states (i.e., +2, +3). For instance, the oxygen vacancies in Cu doped IrO$_2$ can regulate the geometric structure of IrO$_6$ octahedra, which enhances the lift degeneracy of the t_{2g} and e_g orbitals, making the d_{z2} orbital partially occupied and thus weakened binding to oxygen species[46].

3.2 Supported Catalysts

Loading catalytic active Ir species on support can effectively reduce the usage of scarce Ir and enhance overall performance via catalyst/support interaction[77]. However, finding a carrier that combines stability and good conductivity remains a challenge. By calculating Pourbaix diagrams for different elements, Jens K. Nörskov et al.[78] explored the stability of various metal oxides under typical acidic OER conditions and constructed a periodic table of acid-stable elements. They pointed out that oxides containing Sb/Ti/Sn/Ge/Mo/W elements have high corrosion resistance in acidic and oxidative environments. In terms of improving the conductivity, efforts have been devoted to creating massive amounts of mobile electrons or holes in stable Sn, Ti and In based oxides. David P. Wilkinson et al.[79] studied Cr, Fe or V doped Ti_4O_7 and found that V and Fe doped materials have improved conductivity while V doped elements also have better anode stability. The authors believe that the improvement in the stability of V doped materials is mainly because the presence of V can stably improve the conductivity of O vacancies, which makes the material have both good stability and conductivity. Hui Xu et al.[80] compared the conductivity and stability of different types of carriers, and found that the W doped TiO$_2$ carrier maintained good stability, while the conductivity was also greatly improved. The W doped TiO$_2$ was used as a carrier to support a lower loading of Ir, which showed better catalytic activity and stability (Figure 10a, b).

In addition to developing suitable supports, tremendous efforts have also been devoted to rationalizing the performance reinforcement, with a special focus on the catalyst/support interface. To date, the high intrinsic activity and stability of supported catalysts are mainly attributed to the electronic structure regulation induced by lattice strain and direct electron transfer between Ir species and supports. For instance, Ji Yang et al.[55] directly grew IrO$_2$ nanoparticles on the special exposed surface of α-MnO$_2$ nanorods, which produced lattice strain at the two phase interface (Figure 10c). According to their study, the lattice strain enables the adjustment of the band structure of Ir oxides, which is beneficial to the adsorption of intermediate oxygen species and is responsible for the improved catalytic performance. Similar to lattice mismatch, electron transfer can also modulate the electronic structure of Ir species. We recently extend TiN to act as the support for IrO$_2$@Ir nanoparticles (IrO$_2$@Ir/TiN) and applied for OER in acidic media[54]. Combined with DFT simulation, we revealed a direct 2.35 e$^-$ transfer from the TiN (100) surface to the IrO$_2$ cluster, downshifting the d-band center of Ir (E_d = -3.14 eV) from the Fermi level. This electron donation not only weakens the adsorption strength of oxygen species, but also inhibits the dissolution of Ir species

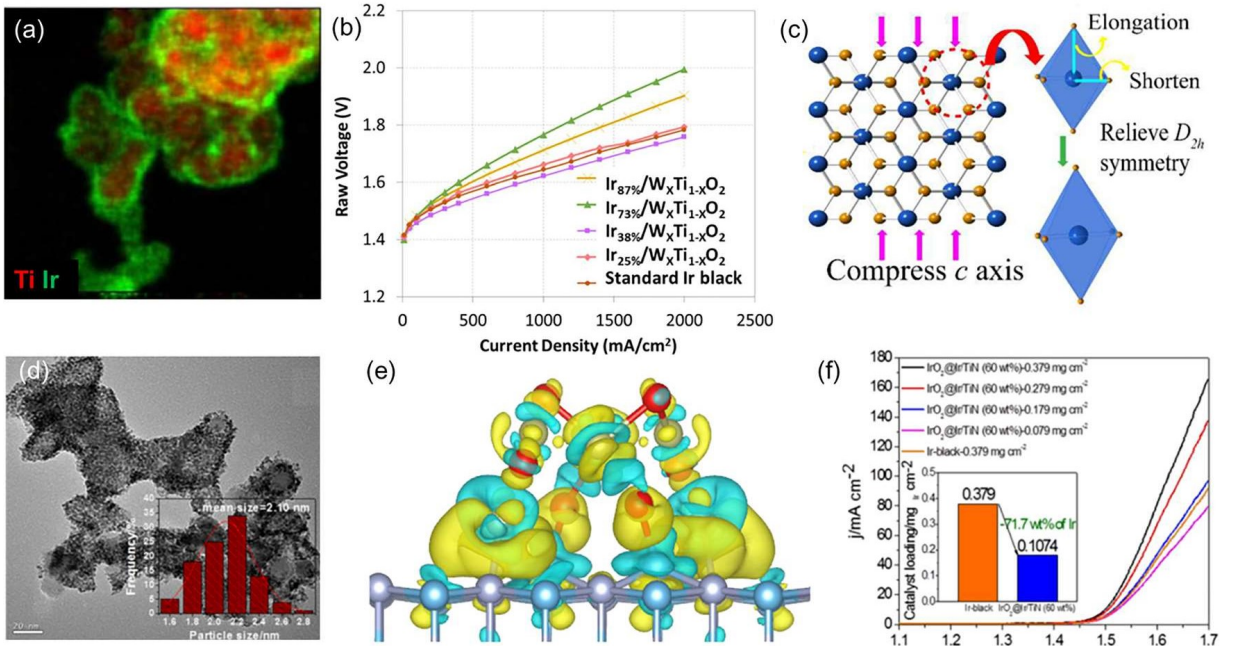

Figure 10 (a) EDS elemental map of Ir38%/$W_xTi_{1-x}O_2$ (Ti = red; Ir = green); (b) Single cell MEA performance in electrolyzers (without *iR* correction). Reprinted from Ref.[81], Copyright 2018, The Electrochemical Society. (c) Diagram showing the process of α-MnO_2 substrate induces the lattice strain of IrO_2. Reprinted with permission from Ref.[55], Copyright 2017, American Chemical Society. (d) TEM image (the inset shows the particle size distribution histogram) of IrO_2@Ir/TiN; (e) Charge-density distribution of the IrO_2/TiN model, the yellow and cyan regions refer to the increased and decreased charge distributions, respectively; (f) LSV curves (without *iR* correction) of IrO_2@Ir/TiN (60 wt%) and Ir black with different catalyst loadings. Reprinted with permission from Ref.[54], Copyright 2018, American Chemical Society. (color on line)

via avoiding the Ir from over-oxidation. The optimal IrO_2@Ir/TiN electrode thus needs only 266 mV overpotential to drive current density of 10 mA·cm^{-2}. Excitingly, as high as 71.7wt% of Ir metal is saved to compete with the commercial Ir-black counterpart (Figure 10d-f).

3.3 Spatially Structured Catalysts

Catalysts with special spatial structures (such as nanoframes[82], nanowires[45], nanosheets[61], porous structures[59], etc.) can expose more active sites, thus greatly improving the atomic utilization of Ir, making it an effective strategy to achieve low Ir usage in PEMWE. For example, we reported a nanoporous IrO_2 catalyst (IrO_2 (1:100)-450 °C) with the highest surface area, ever the reported at 363.3 m^2·g^{-1} was constructed via a facile and efficiently scaled up (up to kilograms) ammonia-induced pore-forming method[59]. Bimodal micro/meso-pores were created all at once without the presence of templates (Figure 11a, b). Attributing to the mass exposed active sites, the overpotential to attain current density at 10 mA·cm^{-2} for water oxidation is only 282 mV for the IrO_2 (1:100)-450 °C catalyst (Figure 11c). Moreover, the overall voltage to achieve current density at 1000 mA·cm^{-2} in a water electrolysis cell is only 1.649 V for IrO_2 (1:100)-450 °C with an Ir loading of 1.71 mg·cm^{-2}, making it highly attractive for application in water electrolysis cell (Figure 11d).

In addition to increasing the atomic utilization of Ir, special spatial configurations are often accompanied by some unique bulk and surface properties. For instance, Fan et al. recently reported 3R-phase IrO_2 2D nanosheets prepared by microwave-assisted mechano-thermal method[63] (Figure 11e, f). The constructed 3R-IrO_2 single unit consists of three layers of IrO_6 octahedra, with six edge-sharing IrO_6 octahedra surrounding each IrO_6 octahedron in each layer, which is distinctive from that of rutile IrO_2 with two

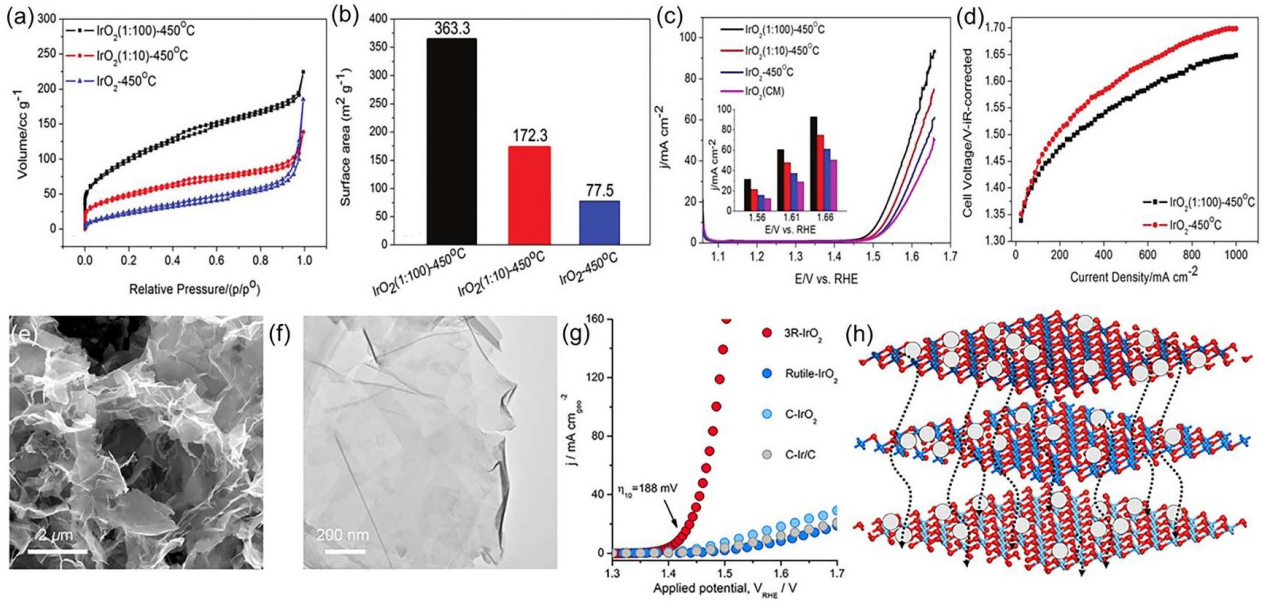

Figure 11 (a) N_2 adsorption/desorption isotherms, and (b) BET specific surface areas of IrO_2 (1:100)-450 °C and the controls; (c) LSV curves recorded at a scanning rate of 5 mV·s^{-1} (the inset shows the current densities at different applied voltages); (d) Steady-state polarization curves of PEMWE cells with *iR* correction. Reprinted from Ref.[59], Copyright 2017, Royal Society of Chemistry. (e, f) SEM and TEM images of 3R-IrO_2, representing the ultrathin morphology; (g) The OER polarization curves of 3R-IrO_2, rutile-IrO_2, C-IrO_2, and C-Ir/C with *iR*-correction; (h) The proton transportation pathway along intralayers in 3R-IrO_2. Reprinted with permission from Ref.[63], Copyright 2021, Elsevier. (color on line)

corners and two edge-sharing IrO_6. Besides, considering that the Ir atoms are buried under oxygen atoms in 3R-IrO_2, appropriate adsorption of hydroxyl and easy desorption are expected, which provide a completely new catalytic surface as Ir atoms on the surface of rutile-IrO_2 are relatively exposed (Figure 11g). Further, combined with the computational method and electrochemical test, they claim that the distinct layered structure will provide suitable channels for protons (H^+) to diffuse freely (Figure 11h), which may show significant advantages for reducing mass transfer resistance in PEMWE devices.

3.4 Single Site Catalysts

Single-atom catalysts have the characteristics of high dispersion of active metal sites, which can achieve the highest utilization rate of active sites, thereby reducing the number of catalysts and becoming one of the focuses of current research on low-Ir catalysts. The strong support interactions and coordination environment effects endow single-site catalysts with various unique properties. The monodisperse feature can also maximize the modulation effect on the catalytic active site[35]. To date, the design of single-site catalysts mainly includes optimizing the electronic structure of the active site under the AEM mechanism and shifting the reaction mechanism to LOM. For example, Qiao et al.[64] constructed a Co_3O_4 supported Ir single-atom catalyst by a process of ion exchange-pyrolysis. Based on a detailed analysis of the location distribution of Ir sites and the catalytic performance, they proposed that short-range ordered Ir single-atom sites exhibit higher catalytic activity (Figure 12a). Combined with theoretical simulation, they claimed that the increase in the number of short-range ordered single Ir sites is correlated with the down-shift of the d-band center (Figure 12b), which is favorable for regulating the oxygen intermediates adsorption energy and contributes to the greatly enhanced OER activity. In addition to the property of support, the dynamic-coupling oxygen legend at highly anodic environment can also affect the electronic structure of Ir. As reported by Su et al., the

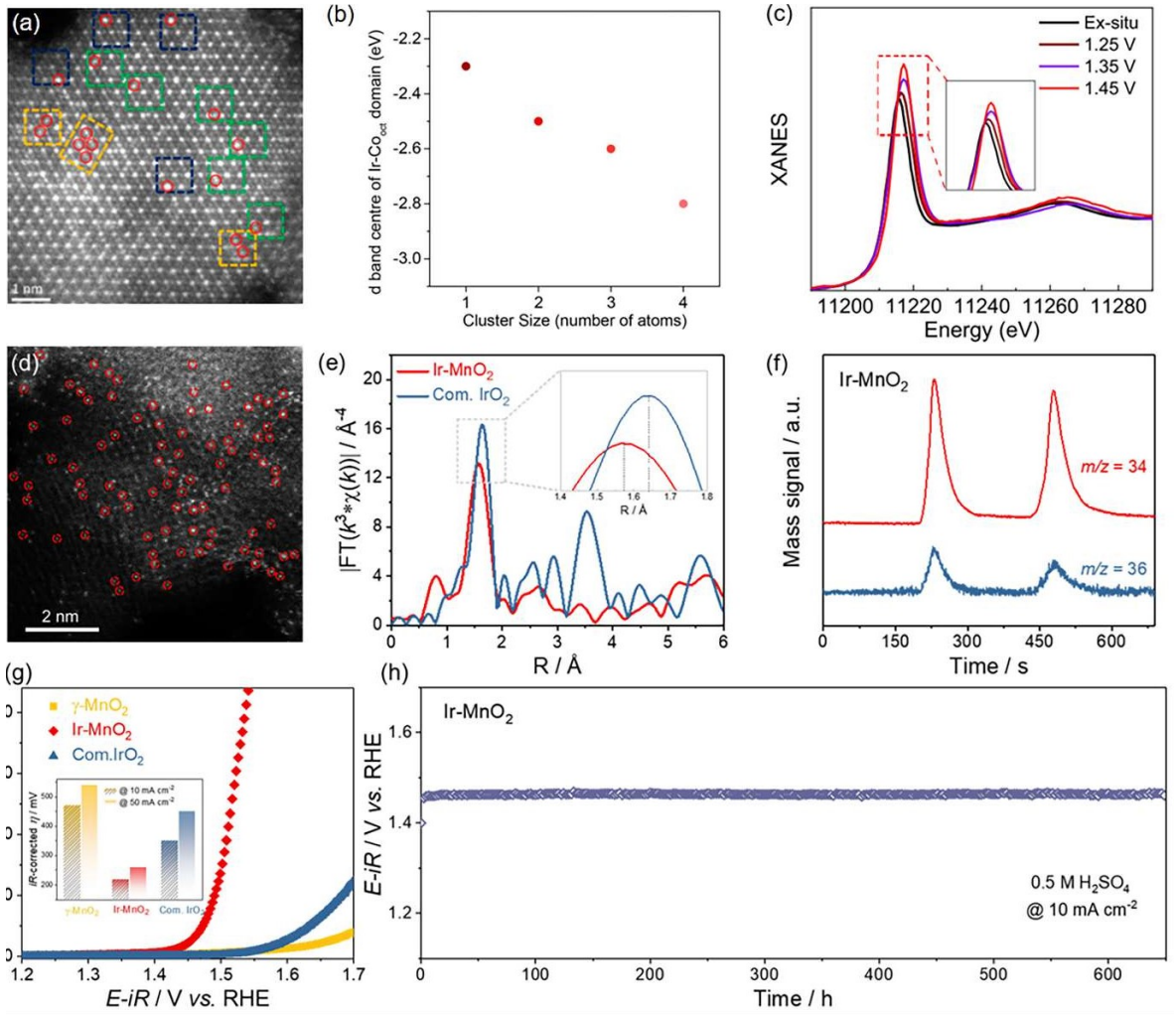

Figure 12 (a) Atomic-resolution HAADF-HRSTEM image of $Ir_{0.06}Co_{2.94}O_4$; (b) The d-band center for configurations with different numbers of short-range ordered single Ir sites. Reprinted from Ref.[64], Copyright 2021, American Chemical Society. (c) *In situ* XANES spectra recorded at the Ir L_3-edge of AD-HN-Ir electrocatalyst at different applied potentials from 1.25 to 1.45 V during OER. Reprinted with permission from Ref.[67], Copyright 2021, American Chemical Socitey. (d) High-magnification HAADF-STEM image of Ir-MnO_2, in which the bright spots highlighted by the red circles are ascribed to Ir single atoms; (e) Fourier-transforms of k^3-weight Ir L_3-edge EXAFS spectra for Ir-MnO_2 and commercial IrO_2; (f) DEMS measurements of $^{16}O^{18}O$ and $^{18}O^{18}O$ signals from the reaction products for ^{18}O-labeled Ir-MnO_2 in 0.5 mol·L^{-1} H_2SO_4 in $H_2{}^{16}O$; (g) LSV curves of Ir-MnO_2, and the controls in 0.5 mol·L^{-1} H_2SO_4. Insert shows the corresponding overpotentials at 10 and 50 mA·cm^{-2}; (h) Chronopotentiometric response of Ir-MnO_2 for OER at 10 mA·cm^{-2}. Reprinted with permission from Ref.[65], Copyright 2021, Elsevier. (color on line)

generation of one oxygen atom at the Ir active site[67], which can be captured by the *in situ* synchrotron radiation infrared and X-ray absorption spectroscopies (Figure 12c), accelerated the transfer of electrons from the metal sites to neighboring atoms toward faster reaction kinetics.

Apart from optimizing the activity to the apex of the AEM volcano plot, shifting the reaction mechanism to LOM with higher theoretical activity is also of interest and has been achieved in our group. Via a simple process of thermal decomposition, we developed a single site Ir doped MnO_2 (Ir-MnO_2)[65] (Figure 12d). The accommodation of Ir atoms into MnO_2 led to approximately 5% Ir-O bond length shrinkage, and thus stronger Ir-O hybridization and easier lattice oxygen redox (Figure 12e). Therefore, the lattice oxy-

gen mediate mechanism is successfully activated, as evidenced by the ^{18}O-labelled DEMS (Figure 12f). More importantly, we argued that the LOM is switched on in a way that only a small fraction of O that bounded to Ir (0.87_{atom}%) are activated, while the rest vast majority of oxygen atoms stay inert. The precise and isolated activation of lattice oxygen oxidation thereby alleviates the oxygen migration and formation of excessive oxygen vacancies, thus ensuring the stabilized LOM performance. As a result, the as-prepared Ir-MnO_2 exhibited excellent activity, i.e., an over 42 times mass activity (766 $A \cdot g_{Ir}^{-1}$) and 359 times TOF (7.9 s^{-1}) that of commercial IrO_2 at an overpotential of 300 mV were achieved (Figure 12g). Moreover, the unprecedented stability of Ir-MnO_2 (with only 15 mV increasement in overpotential after 650 h durability test at 10 $mA \cdot cm^{-2}$) was also uncovered (Figure 12h), outperforming most of the reported electrocatalysts for acidic OER.

4 Evaluation Criteria for Operational Stability

As the stability is a key parameter that must be considered in catalyst design, it is important to establish standardized stability evaluation metrics, and use widely recommended and accepted testing methods to estimate the durability and lifetime of catalysts. In this part, we will first introduce the commonly used indicators for catalyst stability evaluation, and then summarize the widely accepted deactivation characterization techniques. Finally, we will focus on the testing methods of the catalyst lifetime, hoping to provide guidance and advice on relevant representations and tests.

4.1 Stability Evaluation Parameters

In most previous studies, the stability of catalysts is often assessed by measuring the operation time, the overpotential increasing rate at constant current, or the current decay rate at a fixed potential. However, these data are highly susceptible to conditions such as electrode loading, back electrode type, applied potential, etc., making direct comparisons between different catalysts relatively difficult[83]. Therefore, two new evaluation metrics, namely the stability number (S-number)[33] and activity-stability factor (ASF)[84], are proposed and recognized now.

The *S*-number is defined as the ratio between the amount of O_2 generated and the amount of dissolved active metal based on Equation 7.

$$\text{S-number} = \frac{nO_{2(OER)}}{n_{Ir(dissolved)}} \tag{7}$$

It describes how many O_2 molecules are formed per active metal atom dissolved in the electrolyte. The larger the S-number, the better the stability and activity of the OER catalyst[33].

Similar to S-number, the ASF proposed by Kim et al.[84] can be calculated from Equation 8, representing the ratio between the OER current density (j) and the dissolution current density (S), where j is the overall current density including current density derived from OER and anode dissolution, S is the current density of anode dissolution during OER, and η is the applied potential

$$\text{ASF} = \frac{j - S}{S}\Big|\eta \tag{8}$$

The introductions of S-number and ASF enable quantitative description of the stability of catalyst, thus making it more reasonable to compare the durability of different types of catalysts. However, recent studies have shown that the S-number can also be affected by the pH of electrolyte, operational time, catalyst loading and test scenario (in three-electrode or single cell), etc. Thus, when doing catalyst screening, it is necessary to control consistent test conditions.

4.2 Deactivation Characterization Techniques

Structural stability, namely the acid oxidation resistance, is an important indicator of catalyst stability, and can be predicted that structurally unstable catalysts can hardly exhibit good durability under the harsh anode oxygen evolution environment. Therefore, the characterization of catalyst structural stability is an important aspect of stability assessment. In terms of acid stability, immersion of samples in acidic solutions by monitoring the dissolution is the most common method. Some unstable components, such as Fe, Co, Ni, and alkali metals and alkaline

earth metals in perovskite and pyrochlore, may be significantly dissolved in acid, which not only will lead to catalyst destruction, but also may poison the proton exchange membrane in the PEMWE, or even penetrate and deposit to the cathode, resulting in the contamination of the catalyst for the hydrogen evolution reaction. In addition to acid stability, more attention was paid to the stability of catalysts at high oxidation potentials. It is widely recognized that the differences in crystal structure, electronic structure and coordination environment of the catalyst before and after stability testing, captured by SEM/TEM/STEM (Figure 13a), XRD (Figure 13b), XPS (Figure 13c), Raman spectroscopy, XAS (Figure 13d) and other techniques, are of vital importance in evaluating the stability[33]. In addition, *in situ* probing techniques such as *in situ* Raman, *in situ* XAS (Figure 13e), *in situ* ICP[11] (Figure 13f), electrochemical quartz microcrocry stalline balance, DEMS, and etc., are getting more attention as the structure and composition changes at high oxidation potentials can be monitored in real-time.

4.3 Electrochemical Test Methods for Stability

Chronoamperometry (CA) at a constant potential, chronopotentiometry (CP) at a constant current and cyclic voltammetry (CV) in the Faraday zone have been widely used to evaluate the stability for many years[38]. Though direct information on the operational stability of catalysts can be obtained, it is still a challenge to bring the test conditions closer to the actual operating environment of PEMWE (i.e., high anodic

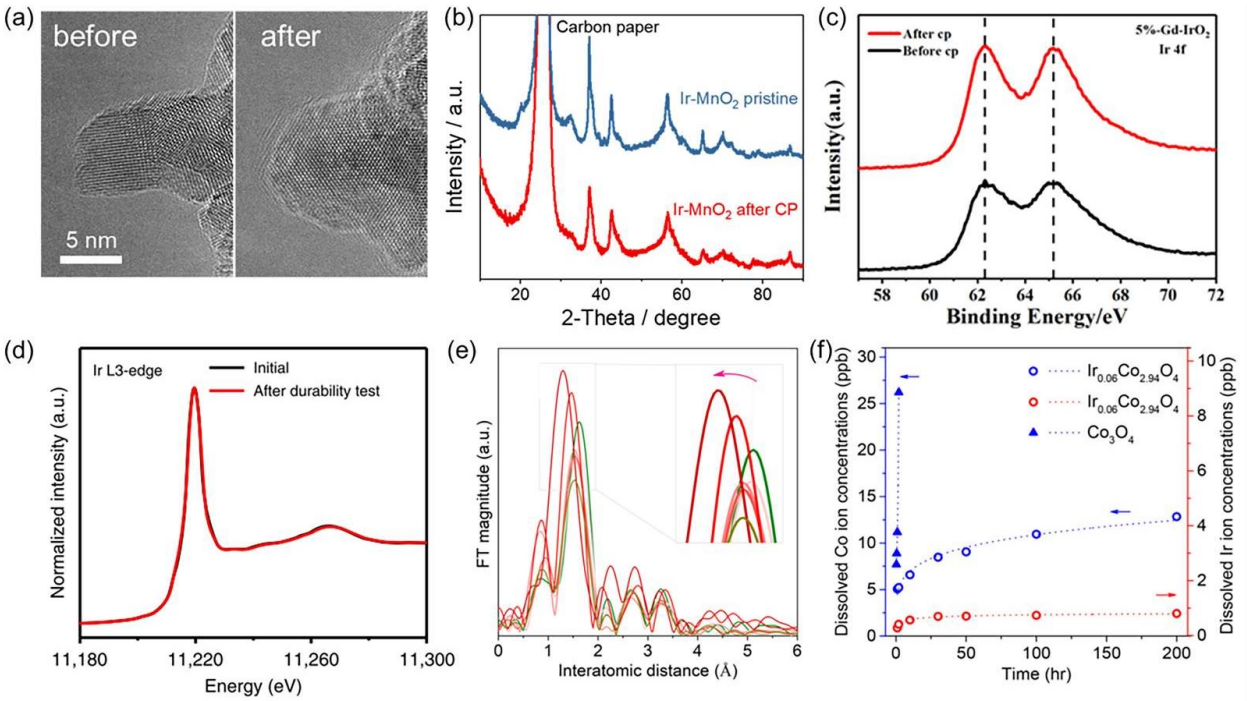

Figure 13 (a) HRTEM images of Ir-MnO_2 before and after chronopotentiometric test, no surface amorphization can be seen; (b) XRD patterns of Ir-MnO_2 before and after chronopotentiometric test, no structure evolution can be observed. Reprinted with permission from Ref.[65] Copyright 2021, Elsevier. (c) High-resolution XPS spectra of Ir 4f for 5%-Gd-pIrO_2 before and after stability test. Reprinted with permission from Ref.[51] , Copyright 2021, American Chemical Society. (d) *Ex situ* XANES spectra of amorphous Ir NSs before and after 8 h durability test. Reprinted with permission from Ref.[85], Copyright 2019, Springer Nature: Nature Communications. (e) *In situ* EXAFS spectra of Li-IrO_x, structure recovering after OER test can be observed. Reprinted with permission from Ref.[86], Copyright 2019, American Chemical Society. (f) The dissolved Co (left-y axis) and Ir (right-y axis) ion concentrations measured for $Ir_{0.06}Co_{2.94}O_4$ (hollow points) and Co_3O_4 (solid points) in electrolyte by ICP-MS. Reprinted with permission from Ref.[64], Copyright 2021, American Chemical Society. (color on line)

potential, volatility power input, high current output, and frequent start and stop) both in three-electrode setup and single cell. Very recently, Alia et al. investigated the effect of different test modes, including constant potential, triangular wave cycling, square wave cycling, sawtooth up cycling and sawtooth down cycling, etc., on the performance degradation of commercial iridium oxide in single cells[87] (Figure 14a-c). Based on the result, they found that frequent potential changes can dramatically accelerate catalyst performance decay. Moreover, they also performed an extended MEA operation with volatility input between 1.45 V and 2.25 V to mimic wind/solar-coupled water electrolysis for 90 days (Figure 14d, e), which provide deeper insights into catalyst stability variation trend. Therefore, we believe that the fluctuating potential cycling is more practical for catalysts that show good stability under constant potential.

5 Future Outlooks

In summary, we have discussed the recent development of low-Ir acidic OER catalysts from the aspects of reaction mechanism, material design, and stability characterization, with a special focus on how to construct low-Ir electrocatalysts with high performance. Although different types of low-Ir catalysts have been reported and exhibited excellent performances in three-electrode setups, the catalyst design concept that matches the requirements of high oxi-

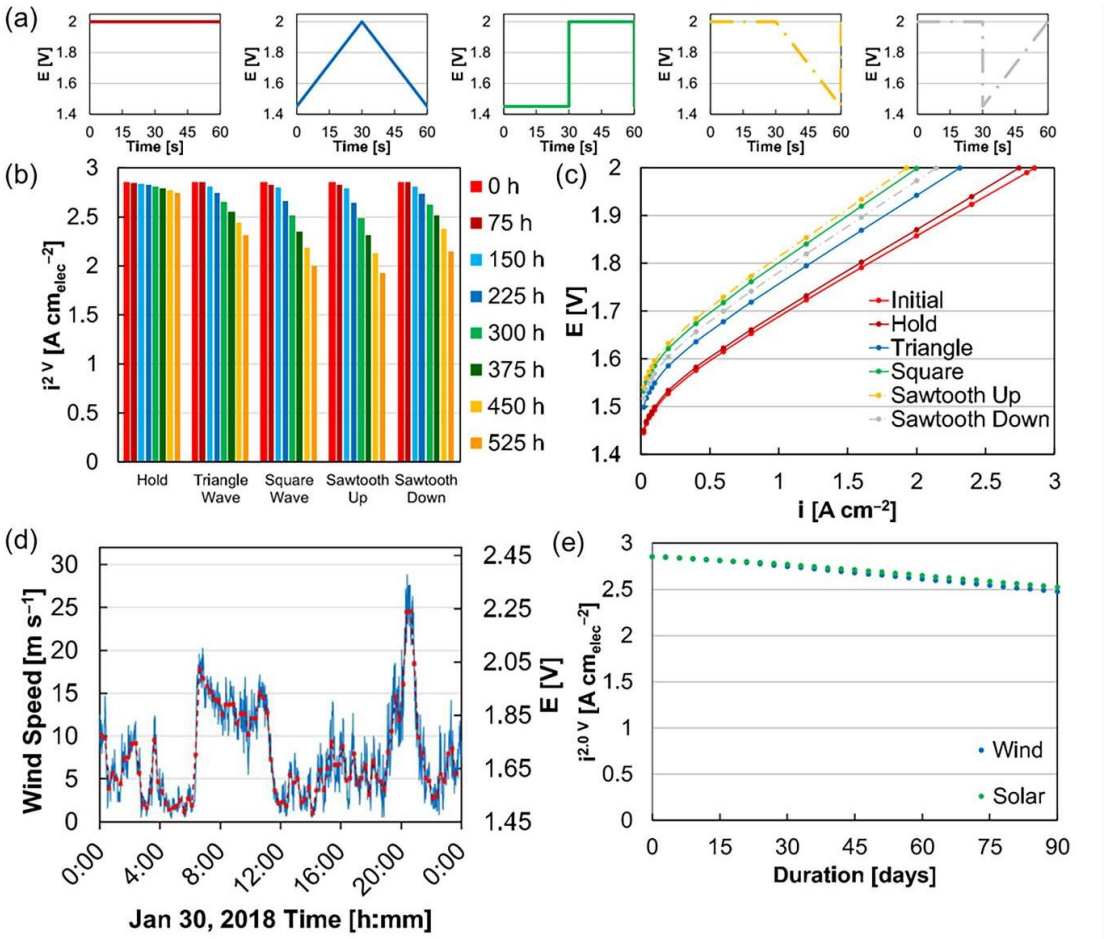

Figure 14 (a) Potential hold, triangle-wave, square-wave, sawtooth up, and sawtooth down profiles applied during MEA testing; (b) Comparison of MEA performance at 2 V during various stability testing modes for 525 h, (c) Comparisons of an initial MEA polarization curve (red) and polarization curves following extended operation; (d) Model wind profile with corresponding potential applied during extended MEA operation; (e) Comparison of MEA performance at 2 V with wind (blue) and solar (green) profiles. Reprinted from Ref.[87], Copyright 2019, The Electrochemical Society. (color on line)

dation portential (usually >1.7 V), high current density (1.5 ~ 2 A·cm^{-2}), long-term operation (> 80,000 h) and low noble metal usage (< 50 $\mu g_{Ir} \cdot cm^{-2}$) under practical PEMWE conditions[88] has not yet been proposed. Some of the challenges related to the design and application of low-Ir electrocatalysts have been highlighted below. Firstly, exploring strategies to stabilize low-Ir catalysts, especially in the condition of fluctuating potential, is imminent as extending the working time can effectively reduce the stack cost. However, most of the current mechanistic studies are centered on activity expression, and less attention is paid to stability. Secondly, electron conductivity needs to be considered in the design of low-Ir catalysts as the ohmic resistance of the catalyst will significantly increase the cell voltage, resulting in higher electricity costs for hydrogen production. Despite the high intrinsic activity of Ir in Ir-based perovskite and pyrochlore, the disappointing conductivity greatly limits its application in PEMWE. Thirdly, evaluating the performance of the developed catalyst in scalable PEMWE devices is necessary. Although a large number of low-Ir catalysts have been developed, most of their performances are based on three-electrode setups, and their performance in single cells is still unknown, which will be detrimental to the practical application of low-Ir catalysts.

Acknowledgements:

Authors wish to thank the National Key R&D Program of China (2020YFB1506800), the National Natural Science Foundation of China (21633008, U1601211, 21733004), the Strategic Priority Research Program of the Chinese Academy of Sciences (XDA21090400), the Jilin Province Science and Technology Development Program (20190201300JC, 20170520150JH, 20200201001JC), Dalian National Laboratory for Clean Energy (DNL), CAS, the Research Innovation Fund (grant DNL202010) for financial supports.

References:

[1] Lagadec M F, Grimaud A. Water electrolysers with closed and open electrochemical systems[J]. Nat. Mater., 2020, 19 (11): 1140-1150.

[2] Zheng Y R, Vernieres J, Wang Z B, Zhang K, Hochfilzer D, Krempl K, Liao T W, Presel F, Altantzis T, Fatermans J, Scott S B, Secher N M, Moon C, Liu P, Bals S, Van Aert S, Cao A, Anand M, Norskov J K, Kibsgaard J, Chorkendorff I. Monitoring oxygen production on mass-selected iridium-tantalum oxide electrocatalysts[J]. Nat. Energy, 2022, 7(1): 55-64.

[3] Seitz L C, Dickens C F, Nishio K, Hikita Y, Montoya J, Doyle A, Kirk C, Vojvodic A, Hwang H Y, Norskov J K, Jaramillo T F. A highly active and stable $IrO_x/SrIrO_3$ catalyst for the oxygen evolution reaction[J]. Science, 2016, 353 (6303): 1011-1014.

[4] Lin C, Li J L, Li X P, Yang S, Luo W, Zhang Y J, Kim S H, Kim D H, Shinde S S, Li Y F, Liu Z P, Jiang Z, Lee J H. *In-situ* reconstructed Ru atom array on α-MnO_2 with enhanced performance for acidic water oxidation[J]. Nat. Catal., 2021, 4(12): 1012-1023.

[5] Shi Z P, Wang X, Ge J J, Liu C P, Xing W. Fundamental understanding of the acidic oxygen evolution reaction: mechanism study and state-of-the-art catalysts[J]. Nanoscale, 2020, 12(25): 13249-13275.

[6] Hegge F, Lombeck F, Cruz Ortiz E, Bohn L, von Holst M, Kroschel M, Hübner J, Breitwieser M, Strasser P, Vierrath S. Efficient and stable low iridium loaded anodes for PEM water electrolysis made possible by nanofiber interlayers [J]. ACS Appl. Energy Mater., 2020, 3(9): 8276-8284.

[7] Park S A, Kim K S, Kim Y T. Electrochemically activated iridium oxide black as promising electrocatalyst having high activity and stability for oxygen evolution reaction[J]. ACS Energy Lett., 2018, 3(5): 1110-1115.

[8] Dickens C F, Nörskov J K. A Theoretical Investigation into the role of surface defects for oxygen evolution on RuO_2 [J]. J. Phys. Chem. C, 2017, 121(34): 18516-18524.

[9] Rong X, Parolin J, Kolpak A M. A fundamental relation ship between reaction mechanism and stability in metal oxide catalysts for oxygen evolution[J]. ACS Catalysis, 2016, 6(2): 1153-1158.

[10] Kasian O, Geiger S, Stock P, Polymeros G, Breitbach B, Savan A, Ludwig A, Cherevko S, Mayrhofer K J J. On the origin of the improved ruthenium stability in RuO_2-IrO_2 mixed oxides[J]. J. Electrochem. Soc., 2016, 163(11): F3099-F3104.

[11] Cherevko S, Geiger S, Kasian O, Kulyk N, Grote J P, Savan A, Shrestha B R, Merzlikin S, Breitbach B, Ludwig A, Mayrhofer K J J. Oxygen and hydrogen evolution reactions on Ru, RuO_2, Ir, and IrO_2 thin film electrodes in acidic and alkaline electrolytes: a comparative study on

activity and stability[J]. Cataly. Today, 2016, 262: 170-180.

[12] Binninger T, Mohamed R, Waltar K, Fabbri E, Levecque P, Kotz R, Schmidt T J. Thermodynamic explanation of the universal correlation between oxygen evolution activity and corrosion of oxide catalysts[J]. Sci. Rep., 2015, 5: 12167.

[13] Cherevko S, Zeradjanin A R, Topalov A A, Kulyk N, Katsounaros I, Mayrhofer K J J. Dissolution of noble metals during oxygen evolution in acidic media[J]. ChemCatChem, 2014, 6(8): 2219-2223.

[14] Danilovic N, Subbaraman R, Chang K C, Chang S H, Kang Y J, Snyder J, Paulikas A P, Strmcnik D, Kim Y T, Myers D, Stamenkovic V R, Markovic N M. Activity-stability trends for the oxygen evolution reaction on monometallic oxides in acidic environments[J]. J. Phys. Chem. Lett., 2014, 5(14): 2474-2478.

[15] Man I C, Su H Y, Calle-Vallejo F, Hansen H A, Martínez J I, Inoglu N G, Kitchin J, Jaramillo T F, Nörskov J K, Rossmeisl J. Universality in oxygen evolution electrocatalysis on oxide surfaces[J]. ChemCatChem, 2011, 3(7): 1159-1165.

[16] Reier T, Nong H N, Teschner D, Schlögl R, Strasser P. Electrocatalytic oxygen evolution reaction in acidic environments-reaction mechanisms and catalysts[J]. Adv. Energy Mater., 2017, 7(1): 1601275.

[17] Koper MTM. Theory of multiple proton-electron transfer reactions and its implications for electrocatalysis[J]. Chem. Sci., 2013, 4(7): 2710-2723.

[18] Koper M T M. Thermodynamic theory of multi-electron transfer reactions: implications for electrocatalysis[J]. J. Electroanal. Chem., 2011, 660(2): 254-260.

[19] Rossmeisl J, Logadottir A, Nörskov J K. Electrolysis of water on (oxidized) metal surfaces[J]. Chem. Phys., 2005, 319(1-3): 178-184.

[20] Dau H, Limberg C, Reier T, Risch M, Roggan S, Strasser P. The mechanism of water oxidation: from electrolysis via homogeneous to biological catalysis[J]. ChemCatChem, 2010, 2(7): 724-761.

[21] Li A, Kong S, Guo C, Ooka H, Adachi K, Hashizume D, Jiang Q, Han H, Xiao J, Nakamura R. Enhancing the stability of cobalt spinel oxide towards sustainable oxygen evolution in acid[J]. Nat. Catal., 2022, 5(2): 109-118.

[22] Fabbri E, Habereder A, Waltar K, Kötz R, Schmidt T J. Developments and perspectives of oxide-based catalysts for the oxygen evolution reaction[J]. Catal. Sci. Technol., 2014, 4(11): 3800-3821.

[23] Mefford J T, Rong X, Abakumov A M, Hardin W G, Dai S, Kolpak A M, Johnston K P, Stevenson K J. Water electrolysis on $La_{1-x}Sr_xCoO_{3-\delta}$ perovskite electrocatalysts [J]. Nat. Commun., 2016, 7: 11053.

[24] Yoo J S, Rong X, Liu Y, Kolpak A M. Role of lattice oxygen participation in understanding trends in the oxygen evolution reaction on perovskites[J]. ACS Catal., 2018, 8(5): 4628-4636.

[25] Grimaud A, Diaz-Morales O, Han B, Hong W T, Lee Y L, Giordano L, Stoerzinger K A, Koper M T M, Shao-Horn Y. Activating lattice oxygen redox reactions in metal oxides to catalyse oxygen evolution[J]. Nat. Chem., 2017, 9 (5): 457-465.

[26] Song F, Busch M M, Lassalle-Kaiser B, Hsu C S, Petkucheva E, Bensimon M, Chen H M, Corminboeuf C, Hu X. An unconventional iron nickel catalyst for the oxygen evolution reaction[J]. ACS Cent. Sci., 2019, 5(3): 558-568.

[27] Yoo J S, Rong X, Liu Y, Kolpak A M. Role of lattice oxygen participation in understanding trends in the oxygen evolution reaction on perovskites[J]. ACS Catal., 2018, 8(5): 4628-4636.

[28] Grimaud A, Diaz-Morales O, Han B, Hong W T, Lee Y L, Giordano L, Stoerzinger K A, Koper M T M, Shao-Horn Y. Activating lattice oxygen redox reactions in metal oxides to catalyse oxygen evolution[J]. Nat. Chem., 2017, 9 (5): 457-465.

[29] Koper M T M. Theory of multiple proton-electron transfer reactions and its implications for electrocatalysis [J]. Chem. Sci., 2013, 4(7): 2710-2723.

[30] Li A, Ooka H, Bonnet N, Hayashi T, Sun Y, Jiang Q, Li C, Han H, Nakamura R. Stable potential windows for long-term electrocatalysis by manganese oxides under acidic conditions[J]. Angew. Chem.-Int. Edit., 2019, 58 (15): 5054-5058.

[31] Zhang R, Dubouis N, Ben Osman M, Yin W, Sougrati M T, Corte DAD, Giaume D, Grimaud A. A Dissolution/precipitation equilibrium on the surface of iridium-based perovskites controls their activity as oxygen evolution reaction catalysts in acidic media[J]. Angew. Chem. Int. Ed., 2019, 58(14): 4571-4575.

[32] Kasian O, Grote J P, Geiger S, Cherevko S, Mayrhofer K J J. The common intermediates of oxygen evolution and dissolution reactions during water electrolysis on iridium [J]. Angew. Chem. Int. Ed., 2018, 57(9): 2488-2491.

[33] Geiger S, Kasian O, Ledendecker M, Pizzutilo E, Mingers A M, Fu W T, Diaz-Morales O, Li Z, Oellers T, Fruchter L, Ludwig A, Mayrhofer K J J, Koper M T M, Cherevko S. The stability number as a metric for electrocatalyst sta-

bility benchmarking[J]. Nat. Catal., 2018, 1(7): 508-515.

[34] Cao L L, Luo Q Q, Chen J J, Wang L, Lin Y, Wang H J, Liu X K, Shen X Y, Zhang W, Liu W, Qi Z M, Jiang Z, Yang J L, Yao T. Dynamic oxygen adsorption on single-atomic ruthenium catalyst with high performance for acidic oxygen evolution reaction[J]. Nat. Commun., 2019, 10(1): 4849.

[35] Yao Y C, Hu S L, Chen W X, Huang Z Q, Wei W C, Yao T, Liu R R, Zang K T, Wang X Q, Wu G, Yuan W J, Yuan T W, Zhu B Q, Liu W, Li Z J, He D S, Xue Z G, Wang Y, Zheng X S, Dong J C, Chang C R, Chen Y X, Hong X, Luo J, Wei S Q, Li W X, Strasser P, Wu Y E, Li Y D. Engineering the electronic structure of single atom Ru sites via compressive strain boosts acidic water oxidation electrocatalysis[J]. Nat. Catal., 2019, 2(4): 304-313.

[36] Wen Y Z, Chen P N, Wang L, Li S Y, Wang Z Y, Abed J, Mao X N, Min Y M, Dinh C T, De Luna P, Huang R, Zhang L S, Wang L, Wang L P, Nielsen R J, Li H H, Zhuang T T, Ke C C, Voznyy O, Hu Y F, Li Y Y, Goddard W A, Zhang B, Peng H S, Sargent E H. Stabilizing highly active Ru sites by suppressing lattice oxygen participation in acidic water oxidation[J]. J. Am. Chem. Soc., 2021, 143(17): 6482-6490.

[37] Park J, Sa Y J, Baik H, Kwon T, Joo S H, Lee K. Iridium-based multimetallic nanoframe@nanoframe structure: an efficient and robust electrocatalyst toward oxygen evolution reaction[J]. ACS Nano, 2017, 11(6): 5500-5509.

[38] Zeng F, Mebrahtu C, Liao L, Beine A K, Palkovits R. Stability and deactivation of OER electrocatalysts: a review[J]. J. Energy Chem., 2022, 69: 301-329.

[39] Martelli G N, Ornelas R, Faita G. Deactivation mechanisms of oxygen evolviong anodes at high current densities[J]. Electrochim. Acta, 1994, 39(11/12): 1151-1158.

[40] Edgington J, Schweitzer N, Alayoglu S, Seitz L C. Constant change: exploring dynamic oxygen evolution reaction catalysis and material transformations in strontium zinc iridate perovskite in acid[J]. J. Am. Chem. Soc., 2021, 143(26): 9961-9971.

[41] Hayashi T, Bonnet-Mercier N, Yamaguchi A, Suetsugu K, Nakamura R. Electrochemical characterization of manganese oxides as a water oxidation catalyst in proton exchange membrane electrolysers[J]. R. Soc. Open Sci., 2019, 6(5): 190122.

[42] Kirshenbaum M J, Richter M H, Dasog M. Electrochemical water oxidation in acidic solution using titanium diboride (TiB_2) catalyst[J]. ChemCatChem, 2019, 11(16): 3877-3881.

[43] Lu X Y, Zhao C A. Electrodeposition of hierarchically structured three-dimensional nickel-iron electrodes for efficient oxygen evolution at high current densities[J]. Nat. Commun., 2015, 6: 6616.

[44] Angulo A, van der Linde P, Gardeniers H, Modestino M, Fernández Rivas D. Influence of bubbles on the energy conversion efficiency of electrochemical reactors[J]. Joule, 2020, 4(3): 555-579.

[45] Alia S M, Shulda S, Ngo C, Pylypenko S, Pivovar B S. Iridium-based nanowires as highly active, oxygen evolution reaction electrocatalysts[J]. ACS Catal.,2018, 8(3): 2111-2120.

[46] Sun W, Song Y, Gong X Q, Cao L M, Yang J. An efficiently tuned d-orbital occupation of IrO_2 by doping with Cu for enhancing the oxygen evolution reaction activity [J]. Chem. Sci.,2015, 6(8): 4993-4999.

[47] Feng J R, Lv F, Zhang W Y, Li P H, Wang K, Yang C, Wang B, Yang Y, Zhou J H, Lin F, Wang G C, Guo S J. Iridium-based multimetallic porous hollow nanocrystals for efficient overall-water-splitting catalysis[J]. Adv. Mater., 2017, 29(47): 1703798.

[48] Li N, Cai L, Wang C, Lin Y, Huang J Z, Sheng H Y, Pan H B, Zhang W, Ji Q Q, Duan H L, Hu W, Zhang W H, Hu F C, Tan H, Sun Z H, Song B, Jin S, Yan W S. Identification of the active-layer structures for acidic oxygen evolution from 9R-$BaIrO_3$ electrocatalyst with enhanced iridium mass activity[J]. J. Am. Chem. Soc., 2021, 143(43): 18001-18009.

[49] Wang H M, Chen Z N, Wu D S, Cao M N, Sun F F, Zhang H, You H H, Zhuang W, Cao R. Significantly enhanced overall water splitting performance by partial oxidation of Ir through Au modification in core-shell alloy structure [J]. J. Am. Chem. Soc., 2021, 143(12): 4639-4645.

[50] Zhao F, Wen B, Niu W H, Chen Z, Yan C, Selloni A, Tully C G, Yang X F, Koel B E. Increasing iridium oxide activity for the oxygen evolution reaction with hafnium modification[J]. J. Am. Chem. Soc., 2021, 143(38): 15616-15623.

[51] Wang Y B, Hou S, Ma R P, Jiang J D, Shi Z P, Liu C P, Ge J J, Xing W. Modulating crystallinity and surface electronic structure of IrO_2 via gadolinium doping to promote acidic oxygen evolution[J]. ACS Sustain. Chem. Eng., 2021, 9(32): 10710-10716.

[52] Liu X H, Xi S B, Kim H, Kumar A, Lee J, Wang J, Tran N Q, Yang T, Shao X D, Liang M F, Kim M G, Lee H. Restructuring highly electron-deficient metal-metal oxides for boosting stability in acidic oxygen evolution reaction[J]. Nat. Commun., 2021, 12(1): 5676.

[53] Jiang G, Yu H M, Li Y H, Yao D W, Chi J, Sun S C, Shao Z G. Low-loading and highly stable membrane electrode based on an Ir@WO_xNR ordered array for PEM water electrolysis[J]. ACS Appl. Mater. Interfaces, 2021, 13(13): 15073-15082.

[54] Li G Q, Li K, Yang L, Chang J F, Ma R P, Wu Z J, Ge J J, Liu C P, Xing W. Boosted performance of Ir species by employing tin as the support toward oxygen evolution reaction[J]. ACS Appl. Mater. Interfaces, 2018, 10(44): 38117-38124.

[55] Sun W, Zhou Z H, Zaman W Q, Cao L M, Yang J. Rational manipulation of IrO_2 lattice strain on α-MnO_2 nanorods as a highly efficient water-splitting catalyst[J]. ACS Appl. Mater. Interfaces, 2017, 9(48): 41855-41862.

[56] Regmi Y N, Tzanetopoulos E, Zeng G S, Peng X, Kushner D I, Kistler T A, King L A, Danilovic N. Supported oxygen evolution catalysts by design: toward lower precious metal loading and improved conductivity in proton exchange membrane water electrolyzers[J]. ACS Catal., 2020, 10(21): 13125-13135.

[57] Oh H S, Nong H N, Reier T, Gliech M, Strasser P. Oxide-supported Ir nanodendrites with high activity and durability for the oxygen evolution reaction in acid PEM water electrolyzers[J]. Chem. Sci., 2015, 6(6): 3321-3328.

[58] Tackett B M, Sheng W C, Kattel S, Yao S Y, Yan B H, Kuttiyiel K A, Wu Q Y, Chen J G G. Reducing iridium loading in oxygen evolution reaction electrocatalysts using core-shell particles with nitride cores[J]. ACS Catal., 2018, 8(3): 2615-2621.

[59] Li G Q, Li S T, Xiao M L, Ge J J, Liu C P, Xing W. Nanoporous IrO_2 catalyst with enhanced activity and durability for water oxidation owing to its micro/mesoporous structure[J]. Nanoscale, 2017, 9(27): 9291-9298.

[60] Lim J, Park D, Jeon S S, Roh C W, Choi J, Yoon D, Park M, Jung H, Lee H. Ultrathin IrO_2 nanoneedles for electrochemical water oxidation[J]. Adv. Funct. Mater., 2018, 28(4): 1704796.

[61] Jiang B, Guo Y N, Kim J, Whitten A E, Wood K, Kani K, Rowan A E, Henzie J, Yamauchi Y. Mesoporous metallic iridium nanosheets[J]. J. Am. Chem. Soc., 2018, 140(39): 12434-12441.

[62] Dang Q, Lin H P, Fan Z L, Ma L, Shao Q, Ji Y J, Zheng F F, Geng S Z, Yang S Z, Kong N N, Zhu W X, Li Y Y, Liao F, Huang X Q, Shao M W. Iridium metallene oxide for acidic oxygen evolution catalysis[J]. Nat. Commun., 2021, 12(1): 6007.

[63] Fan Z L, Ji Y J, Shao Q, Geng S Z, Zhu W X, Liu Y, Liao F, Hu Z W, Chang Y C, Pao C W, Li Y Y, Kang Z H, Shao M W. Extraordinary acidic oxygen evolution on new phase 3R-iridium oxide[J]. Joule, 2021, 5(12): 3221-3234.

[64] Shan J Q, Ye C, Chen S M, Sun T L, Jiao Y, Liu L M, Zhu C Z, Song L, Han Y, Jaroniec M, Zhu Y H, Zheng Y, Qiao S Z. Short-range ordered iridium single atoms integrated into cobalt oxide spinel structure for highly efficient electrocatalytic water oxidation[J]. J. Am. Chem. Soc., 2021, 143(13): 5201-5211.

[65] Shi Z P, Wang Y, Li J, Wang X, Wang Y B, Li Y, Xu W L, Jiang Z, Liu C P, Xing W, Ge J J. Confined Ir single sites with triggered lattice oxygen redox: toward boosted and sustained water oxidation catalysis[J]. Joule, 2021, 5(8): 2164-2176.

[66] Yin J, Jin J, Lu M, Huang B L, Zhang H, Peng Y, Xi P X, Yan C H. Iridium single atoms coupling with oxygen vacancies boosts oxygen evolution reaction in acid media[J]. J. Am. Chem. Soc., 2020, 142(43): 18378-18386.

[67] Su H, Zhou W L, Zhou W, Li Y L, Zheng L R, Zhang H, Liu M H, Zhang X X, Sun X, Xu Y Z, Hu F C, Zhang J, Hu T D, Liu Q H, Wei S Q. *In-situ* spectroscopic observation of dy namic-coupling oxygen on atomically dispersed iridium electrocatalyst for acidic water oxidation[J]. Nat. Commun., 2021, 12(1): 6118.

[68] Hao S Y, Sheng H Y, Liu M, Huang J Z, Zheng G K, Zhang F, Liu X N, Su Z W, Hu J J, Qian Y, Zhou L N, He Y, Song B, Lei L C, Zhang X W, Jin S. Torsion strained iridium oxide for efficient acidic water oxidation in proton exchange membrane electrolyzers[J]. Nat. Nanotechnol., 2021, 16(12): 1371-1377.

[69] Pi Y C, Shao Q, Wang P T, Guo J, Huang X Q. General formation of monodisperse IrM (M = Ni, Co, Fe) bimetallic nanoclusters as bifunctional electrocatalysts for acidic overall water splitting[J]. Adv. Funct. Mater., 2017, 27(27): 1700886.

[70] Hao S Y, Wang Y H, Zheng G K, Qiu L S, Xu N, He Y, Lei L C, Zhang X W. Tuning electronic correlations of ultra-small IrO_2 nanoparticles with La and Pt for enhanced oxygen evolution performance and long-durable stability in acidic media[J]. Appl. Catal. B, 2020, 266: 118643.

[71] Jin Z Y, Lv J, Jia H L, Liu W H, Li H L, Chen Z H, Lin X, Xie G Q, Liu X J, Sun S H, Qiu H J. Nanoporous Al-Ni-Co-Ir-Mo high-entropy alloy for record-high water splitting activity in acidic environments[J]. Small, 2019, 15(47): e1904180.

[72] Yang L, Yu G T, Ai X, Yan W S, Duan H L, Chen W, Li X T, Wang T, Zhang C H, Huang X R, Chen J S, Zou X

X. Efficient oxygen evolution electrocatalysis in acid by a perovskite with face-sharing IrO_6 octahedral dimers[J]. Nat. Commun., 2018, 9(1): 5236.

[73] Shang C Y, Cao C, Yu D Y, Yan Y, Lin Y T, Li H L, Zheng T T, Yan X P, Yu W C, Zhou S M, Zeng J. Electron correlations engineer catalytic activity of pyrochlore iridates for acidic water oxidation[J]. Adv. Mater., 2019, 31(6): e1805104.

[74] Zhang Q, Liang X, Chen H, Yan W S, Shi L, Liu Y P, Li J Y, Zou X X. Identifying key structural subunits and their synergism in low-iridium triple perovskites for oxygen evolution in acidic media[J]. Chem. Mater., 2020, 32 (9): 3904-3910.

[75] Reier T, Pawolek Z, Cherevko S, Bruns M, Jones T, Teschner D, Selve S, Bergmann A, Nong H N, Schlogl R, Mayrhofer K J J, Strasser P. Molecular insight in structure and activity of highly efficient, low-Ir Ir-Ni oxide catalysts for electrochemical water splitting (OER)[J]. J. Am. Chem. Soc., 2015, 137(40): 13031-13040.

[76] Nong H N, Reier T, Oh H S, Gliech M, Paciok P, Vu T H T, Teschner D, Heggen M, Petkov V, Schlögl R, Jones T, Strasser P. A unique oxygen ligand environment facilitates water oxidation in hole-doped $IrNiO_x$ core-shell electrocatalysts[J]. Nat. Catal., 2018, 1(11): 841-851.

[77] Oh H S, Nong H N, Reier T, Bergmann A, Gliech M, Ferreira de Araujo J, Willinger E, Schlogl R, Teschner D, Strasser P. Electrochemical catalyst-support effects and their stabilizing role for IrO_x nanoparticle catalysts during the oxygen evolution reaction[J]. J. Am. Chem. Soc., 2016, 138(38): 12552-12563.

[78] Wang Z B, Zheng Y R, Chorkendorff I, Nörskov J K. Acid-stable oxides for oxygen electrocatalysis[J]. ACS Energy Lett., 2020, 5(9): 2905-2908.

[79] English J T, Wilkinson D P. The superior electrical conductivity and anodic stability of vanadium-doped Ti_4O_7 [J]. J. Electrochem. Soc., 2021, 168(10): 103509.

[80] Zhao S, Stocks A, Rasimick B, More K, Xu H. Highly active, durable dispersed iridium nanocatalysts for PEM water electrolyzers[J]. J. Electrochem. Soc. ,2018, 165(2): F82-F89.

[81] Zhao S, Stocks A, Rasimick B, More K, Xu H. Highly active, durable dispersed iridium nanocatalysts for PEM water electrolyzers[J]. J. Electrochem. Soc., 2018, 165(2): F82-F89.

[82] Faustini M, Giraud M, Jones D, Rozière J, Dupont M, Porter T R, Nowak S, Bahri M, Ersen O, Sanchez C, Bois sière C, Tard C, Peron J. Hierarchically structured ultraporous iridium-based materials: a novel catalyst architecture for proton exchange membrane water electrolyzers [J]. Adv. Energy Mater., 2019, 9(4): 1802136.

[83] Knoppel J, Mockl M, Escalera-Lopez D, Stojanovski K, Bierling M, Bohm T, Thiele S, Rzepka M, Cherevko S. On the limitations in assessing stability of oxygen evolution catalysts using aqueous model electrochemical cells [J]. Nat. Commun., 2021, 12(1): 2231.

[84] Kim Y T, Lopes P P, Park S A, Lee A Y, Lim J, Lee H, Back S, Jung Y, Danilovic N, Stamenkovic V, Erlebacher J, Snyder J, Markovic N M. Balancing activity, stability and conductivity of nanoporous core-shell iridium/iridium oxide oxygen evolution catalysts[J]. Nat. Commun., 2017, 8(1): 1449.

[85] Wu G, Zheng X S, Cui P X, Jiang H Y, Wang X Q, Qu Y T, Chen W X, Lin Y, Li H, Han X, Hu Y M, Liu P G, Zhang Q H, Ge J J, Yao Y C, Sun R B, Wu Y, Gu L, Hong X, Li Y D. A general synthesis approach for amorphous noble metal nanosheets[J]. Nat. Commun., 2019, 10(1): 4855.

[86] Gao J J, Xu C Q, Hung S F, Liu W, Cai W Z, Zeng Z P, Jia C M, Chen H M, Xiao H, Li J, Huang Y Q, Liu B. Breaking long-range order in iridium oxide by alkali ion for efficient water oxidation[J]. J. Am. Chem. Soc., 2019, 141(7): 3014-3023.

[87] Alia S M, Stariha S, Borup R L. Electrolyzer durability at low catalyst loading and with dynamic operation[J]. J. Electrochem. Soc., 2019, 15(166): F1164-F1172.

[88] Pivovar B. H_2 new: Hydrogen (H_2) from next-generation electrolyzers of water overview[R]. United States: DOE, 2021.

低铱酸性氧析出电催化剂的研究进展

倪 静[1,2#],施兆平[1,2#],王 显[1,2],王意波[1,2],吴鸿翔[1,2],
刘长鹏[1,2*],葛君杰[1,2,3*],邢 巍[1,2*]

(1. 中国科学院长春应用化学研究所,吉林省先进低碳化学电源重点实验室,电分析化学国家重点实验室,
吉林 长春 130022; 2 中国科学技术大学应用化学与工程学院,安徽 合肥,230026;
3. 中国科学院大连洁净能源创新研究院,辽宁 大连 116023)

摘要: 开发高性能、低成本的氧析出反应(OER)电催化剂是促进质子交换膜水电解(PEMWE)制氢规模化应用的关键。迄今为止, OER 催化剂的最佳选项仍为贵金属铱(Ir), 但其仍存在活性不足和储量稀缺的问题, 进而增加了材料成本和电力成本。因此, 开发低 Ir 载量、高活性和稳定性间距, 且能够满足 PEMWE 设备中大电流密度和长期运行要求的 OER 催化剂是十分必要的。这些目标的实现需要深入理解酸性 OER 机制、明晰材料设计方法, 并建立可靠的性能评估指标(特别是对耐久性的评估)。综上,本文首先系统总结了目前被广泛接受的酸性 OER 活性表达机制(即吸附析出机制、晶格氧氧化机制和多活性中心机制)和失活机制(即活性物种溶解、晶相和形态演化、催化剂脱落和活性位点阻塞), 为催化剂的微观结构设计提供指导。其次, 我们讨论了最近报道的几类低铱 OER 催化剂, 包括多金属合金氧化物、负载型催化剂、具有特殊空间结构的催化剂和单位点催化剂, 并重点描述低 Ir 催化剂中的性能如何得以调控以及其中潜在的构效关系。随后, 我们介绍了常用的催化剂稳定性评价指标、催化剂失活表征技术以及模拟 PEMWE 实际操作条件的催化剂寿命测试方法, 希望为催化剂筛选提供依据。最后, 针对未来可用于 PEMWE 体系的低铱 OER 催化剂的探索提出了一些可行建议。

关键词: 氧析出反应;质子交换膜水电解;低铱载量;活性稳定性机制;稳定性评估指标